The homogenization of orthorhombic piezoelectric composites by the strong-property-fluctuation theory

2009 J. Phys. A: Math. Theor. 42 165402

(http://iopscience.iop.org/1751-8121/42/16/165402)

IOP PUBLISHING JOURNAL OF PHYSICS A: MATHEMATICAL AND THEORETICAL

J. Phys. A: Math. Theor. **42** (2009) 165402 (24pp) doi:10.1088/1751-8113/42/16/165402

The homogenization of orthorhombic piezoelectric composites by the strong-property-fluctuation theory

Andrew J Duncan[1], **Tom G Mackay**[1,2] **and Akhlesh Lakhtakia**[2]

[1] School of Mathematics and Maxwell Institute for Mathematical Sciences, University of Edinburgh, Edinburgh EH9 3JZ, UK
[2] NanoMM—Nanoengineered Metamaterials Group, Department of Engineering Science and Mechanics, Pennsylvania State University, University Park, PA 16802–12, USA

E-mail: Andrew.Duncan@ed.ac.uk, T.Mackay@ed.ac.uk and akhlesh@psu.edu

Received 14 November 2008, in final form 9 March 2009
Published 31 March 2009
Online at stacks.iop.org/JPhysA/42/165402

Abstract

The linear strong-property-fluctuation theory (SPFT) was developed in order to estimate the constitutive parameters of certain homogenized composite materials (HCMs) in a long-wavelength regime. The component materials of the HCM were generally orthorhombic $mm2$ piezoelectric materials, which were randomly distributed as oriented ellipsoidal particles. At the second-order level of approximation, wherein a two-point correlation function and its associated correlation length characterize the component material distributions, the SPFT estimates of the HCM constitutive parameters were expressed in terms of numerically tractable two-dimensional integrals. Representative numerical calculations revealed that (i) the lowest order SPFT estimates are qualitatively similar to those provided by the corresponding Mori–Tanaka homogenization formalism, but differences between the two estimates become more pronounced as the component particles become more eccentric in shape, and (ii) the second-order SPFT estimate provides a significant correction to the lowest order estimate, which accommodates attenuation due to scattering losses.

PACS numbers: 78.20.Hp, 77.65.−j, 78.20.Ci

(Some figures in this article are in colour only in the electronic version)

1. Introduction

Since piezoelectric materials can convert electrical energy to mechanical energy, and vice versa, they are of considerable technological importance. However, bulk piezoelectric materials commonly exhibit physical properties which render them unsuitable for particular applications. For example, certain ceramics exhibit strong piezoelectric properties but their weight, malleability and acoustic impedance are not suitable for transducer applications [1].

Accordingly, composite piezoelectric materials are often more technologically attractive [2], and these can be found in a host of applications such as in transducers, sensors, actuators and energy harvesting devices, for example [3, 4]. Furthermore, the recent proliferation of multi-functional metamaterials [5]—which often take the form of homogenized composite materials (HCMs), exhibiting exotic constitutive properties [6]—presents interesting possibilities for piezoelectric HCMs.

While the estimation of elastodynamic or electromagnetic constitutive parameters of HCMs is a challenging task, especially for anisotropic HCMs, the estimation of constitutive parameters of piezoelectric HCMs is more challenging due to the coupling of elastodynamic and electromagnetic fields. Numerous homogenization formalisms have been proposed for piezoelectric HCMs, many of which build upon Eshelby's landmark description of the elastodynamic response of a single ellipsoidal particle immersed in an infinite homogeneous medium [7]. For example, the Mori–Tanaka [8–10], self-consistent and differential approaches [11]—and combinations of these [12]—feature prominently in the literature. In the following we present a fundamentally different approach to estimating the constitutive properties of piezoelectric HCMs, based on the strong-property-fluctuation theory (SPFT). A key feature of the SPFT homogenization approach—which distinguishes it from other more conventional approaches—is the accommodation of higher order characterizations of the distributional statistics of the HCM's component materials. This accommodation of higher order statistics enables scattering losses to be taken into account.

The origins of the SPFT lie in wave propagation studies for continuously random media [13]. It was later adapted to estimate the electromagnetic [14–16], acoustic [17] and elastodynamic [18] constitutive parameters of HCMs. Within the SPFT, the estimation of the HCM constitutive parameters arises from the asymptotic expansion of a mass operator. The lowest order term in this expansion is represented by a homogeneous comparison medium. By a renormalization procedure, the SPFT allows for relatively strong fluctuations in the constitutive parameters describing the comparison medium and the component materials. Thus, the SPFT is distinguished from the weak-property-fluctuation theory [13]. Higher order approximations are expressed in terms of correlation functions describing the spatial distributions of the component materials. In principle, correlation functions of arbitrarily high order may be incorporated; but, in practice, the SPFT is most often implemented at the second-order level of approximation, wherein a two-point correlation function and its associated correlation length characterize the component material distributions. Thus, by the introduction of these spatial correlation functions, a spatially nonlocal description is achieved. As the SPFT is developed within the frequency domain, temporal nonlocality is represented by the imaginary parts of complex-valued constitutive parameters.

We establish here the linear, second-order SPFT appropriate to orthorhombic $mm2$ piezoelectric HCMs, arising from component materials which are randomly distributed as oriented ellipsoidal particles. The theoretical development builds upon the corresponding development of the orthotropic elastodynamic SPFT [18, 19]. A representative numerical example is used to illustrate the theory, and results are compared with those from the well-established Mori–Tanaka formalism.

2. Theory

2.1. Preliminaries

In the following, we consider piezoelectric materials described by constitutive relations of the form [20, 21]

$$\left.\begin{aligned} \sigma_{ab} &= C_{abmn} S_{mn} - e_{nab} E_n \\ D_a &= e_{amn} S_{mn} + \epsilon_{an} E_n \end{aligned}\right\}, \tag{1}$$

wherein the elastic strain S_{mn} and the electric field E_n are taken as independent variables, which are related to the stress σ_{ab} and dielectric displacement D_a via the elastic stiffness tensor C_{abmn} (measured in a constant electric field), the piezoelectric tensor e_{nab} (measured at a constant strain or electric field) and the dielectric tensor ϵ_{an} (measured at a constant strain). Here, and hereafter, tensors are represented in plain font and lowercase tensor indexes range from 1 to 3 with a repeated index implying summation.

We develop the SPFT in the frequency domain. Accordingly the complex-valued representations of the stress, strain and electromagnetic fields have an implicit $\exp(-\mathrm{i}\omega t)$ dependence on time t with ω being the angular frequency and $i = \sqrt{-1}$. The possibility of dissipative behavior is thereby accommodated via the imaginary parts of complex-valued constitutive parameters.

The constitutive relations (1) are more conveniently expressed in the symbolic form

$$\breve{\sigma}_{aB} = \breve{C}_{aBMn} \breve{S}_{Mn}, \tag{2}$$

where the extended stress symbol

$$\breve{\sigma}_{aB} = \begin{cases} \sigma_{ab}, & B = b = 1, 2, 3 \\ D_a, & B = 4, \end{cases} \tag{3}$$

the extended stiffness symbol

$$\breve{C}_{aBMn} = \begin{cases} C_{abmn}, & B = b = 1, 2, 3;\ M = m = 1, 2, 3 \\ e_{nab}, & B = b = 1, 2, 3;\ M = 4 \\ -e_{amn}, & B = 4;\ M = m = 1, 2, 3 \\ \epsilon_{an}, & B, M = 4, \end{cases} \tag{4}$$

and the extended strain symbol

$$\breve{S}_{Mn} = \begin{cases} S_{mn}, & M = m = 1, 2, 3 \\ E_n, & M = 4. \end{cases} \tag{5}$$

Here, and hereafter, uppercase indexes range from 1 to 4. Note that the extended quantities defined in equations (3)–(5) are not tensors—these are simply symbols which are introduced to allow a compact representation of the piezoelectric constitutive relations [9].

In developing the SPFT appropriate to piezoelectric HCMs, it is expedient to express the constitutive relations (2) in a matrix vector form as[3]

$$\breve{\boldsymbol{\sigma}} = \underline{\underline{\breve{\mathbf{C}}}} \cdot \breve{\mathbf{S}}, \tag{6}$$

wherein $\breve{\boldsymbol{\sigma}}$ and $\breve{\mathbf{S}}$ are column 12-vectors representing the extended stress and extended strain symbols, respectively, and $\underline{\underline{\breve{\mathbf{C}}}}$ is a 12×12 matrix which represents the extended stiffness symbol. Here, and hereafter, matrixes are denoted by double underlining and bold font, whereas vectors are in bold font with no underlining. For use later on, we note that the pq th entry of a matrix $\underline{\underline{\mathbf{A}}}$ is written as $[\underline{\underline{\mathbf{A}}}]_{pq}$, while the pth entry of a vector $\mathbf{b}$ is written as $[\mathbf{b}]_p$. The adjoint, determinant, inverse, trace and transpose of a matrix $\underline{\underline{\mathbf{A}}}$ are denoted by $\mathrm{adj}(\underline{\underline{\mathbf{A}}})$, $\det(\underline{\underline{\mathbf{A}}})$, $\underline{\underline{\mathbf{A}}}^{-1}$, $\mathrm{tr}(\underline{\underline{\mathbf{A}}})$ and $\underline{\underline{\mathbf{A}}}^T$, respectively. The $n \times n$ null matrix is written as $\underline{\underline{\mathbf{0}}}_{n\times n}$.

Our concern in this paper is with orthorhombic $mm2$ piezoelectric materials [20, 21]. For this symmetry class, the extended stiffness matrix has the block matrix form

$$\underline{\underline{\breve{\mathbf{C}}}} = \begin{pmatrix} \underline{\underline{\mathbf{C}}} & -\underline{\underline{\mathbf{e}}}^T \\ \underline{\underline{\mathbf{e}}} & \underline{\underline{\boldsymbol{\epsilon}}} \end{pmatrix}, \tag{7}$$

[3] This notation is an extension of the Kelvin notation [21].

where the 9×9 stiffness matrix $\underline{\underline{\mathbf{C}}}$ may be expressed as

$$\underline{\underline{\mathbf{C}}} = \begin{pmatrix} \underline{\underline{\mathbf{C}}}_a & \underline{\underline{\mathbf{0}}}_{3\times3} & \underline{\underline{\mathbf{0}}}_{3\times3} \\ \underline{\underline{\mathbf{0}}}_{3\times3} & \underline{\underline{\mathbf{C}}}_b & \underline{\underline{\mathbf{C}}}_b \\ \underline{\underline{\mathbf{0}}}_{3\times3} & \underline{\underline{\mathbf{C}}}_b & \underline{\underline{\mathbf{C}}}_b \end{pmatrix}, \tag{8}$$

with the 3×3 symmetric matrix components

$$\underline{\underline{\mathbf{C}}}_a = \begin{pmatrix} C_{11} & C_{12} & C_{13} \\ C_{12} & C_{22} & C_{23} \\ C_{13} & C_{23} & C_{33} \end{pmatrix}, \qquad \underline{\underline{\mathbf{C}}}_b = \begin{pmatrix} C_{44} & 0 & 0 \\ 0 & C_{55} & 0 \\ 0 & 0 & C_{66} \end{pmatrix}, \tag{9}$$

while the 9×3 piezoelectric matrix $\underline{\underline{\mathbf{e}}}$ may be expressed as

$$\underline{\underline{\mathbf{e}}} = \begin{pmatrix} 0 & 0 & 0 & 0 & e_{15} & 0 & 0 & e_{15} & 0 \\ 0 & 0 & 0 & e_{24} & 0 & 0 & e_{24} & 0 & 0 \\ e_{31} & e_{32} & e_{33} & 0 & 0 & 0 & 0 & 0 & 0 \end{pmatrix} \tag{10}$$

and the 3×3 dielectric matrix $\underline{\underline{\boldsymbol{\epsilon}}}$ as

$$\underline{\underline{\boldsymbol{\epsilon}}} = \begin{pmatrix} \epsilon_{11} & 0 & 0 \\ 0 & \epsilon_{22} & 0 \\ 0 & 0 & \epsilon_{33} \end{pmatrix}. \tag{11}$$

The correspondence between the tensor/extended symbol representation and the matrix-vector representation is described in appendix A.

In an analogous fashion, the material density ρ may be represented via the extended density symbol

$$\breve{\rho}_{BM} = \begin{cases} \rho, & B = M = 1, 2, 3 \\ 0, & \text{otherwise}, \end{cases} \tag{12}$$

which has the 4×4 extended matrix counterpart $\underline{\underline{\breve{\boldsymbol{\rho}}}}$ with entries

$$[\underline{\underline{\breve{\boldsymbol{\rho}}}}]_{MP} = \breve{\rho}_{MP}. \tag{13}$$

2.2. *Component materials*

We consider the homogenization of a composite comprising two component materials, labeled as component material '1' and component material '2'. In general, both components are homogeneous, orthorhombic $mm2$ piezoelectric materials, characterized by the stiffness tensors $C^{(\ell)}_{abmn}$, piezoelectric tensors $e^{(\ell)}_{nab}$, dielectric tensors $\epsilon^{(\ell)}_{an}$ and densities $\rho^{(\ell)}$ $(\ell = 1, 2)$. In conformity with the notational practices introduced in section 2.1, the component materials are also described by the extended stiffness symbols $\breve{C}^{(\ell)}_{aBMn}$ (and their 12×12 matrix equivalents $\underline{\underline{\breve{\mathbf{C}}}}^{(\ell)}$) and extended density symbols $\breve{\rho}^{(\ell)}_{BM}$ (and their 4×4 matrix equivalents $\underline{\underline{\breve{\boldsymbol{\rho}}}}^{(\ell)}$).

The component materials are randomly distributed as identically oriented, conformal, ellipsoidal particles. As a mathematical convenience, the principal axes of the ellipsoidal particles are aligned with the Cartesian axes; more general particle orientations are accommodated through appropriate rotations of the coordinate axes. Thus, the surface of each ellipsoidal particle may be parameterized by the vector

$$\mathbf{r}^{(e)} = \eta \underline{\underline{\mathbf{U}}} \cdot \hat{\mathbf{r}}, \tag{14}$$

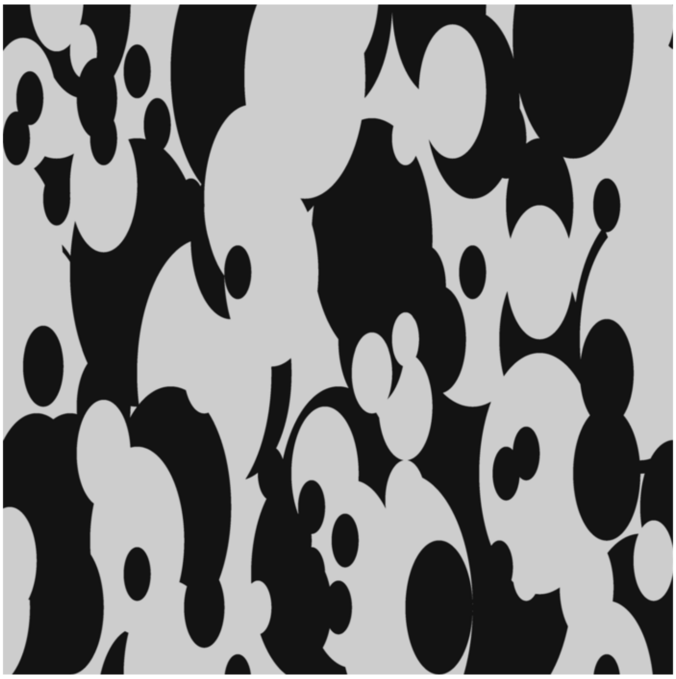

Figure 1. A schematic illustration of a random mixture of two different populations of ellipsoidal particles, sharing the same orientation.

where η is a linear measure of size, $\hat{\mathbf{r}}$ is the radial unit vector and the diagonal shape matrix

$$\underline{\underline{\mathbf{U}}} = \frac{1}{\sqrt[3]{abc}} \begin{pmatrix} a & 0 & 0 \\ 0 & b & 0 \\ 0 & 0 & c \end{pmatrix} \qquad (a, b, c \in \mathbb{R}^+). \tag{15}$$

A wide range of particle shapes are thereby catered for, including spheres ($a = b = c$) and spheroids ($a = b \neq c$), and the limiting cases of very long needles ($a \to 1, b = c \to 0$) and very thin disks ($a = b \to 1, c \to 0$). A schematic illustration of the random mixture of the two component materials is presented in figure 1.

Let V denote the space occupied by the composite material. Then $V = V^{(1)} \cup V^{(2)}$, where $V^{(1)}$ and $V^{(2)}$ contain the two component materials labeled as '1' and '2', respectively, and $V^{(1)} \cap V^{(2)} = \emptyset$. The distributional statistics of the component materials are described in terms of ensemble averages of the characteristic functions

$$\Phi^{(\ell)}(\mathbf{r}) = \begin{cases} 1, & \mathbf{r} \in V^{(\ell)} \\ 0, & \mathbf{r} \notin V^{(\ell)} \end{cases} \qquad (\ell = 1, 2). \tag{16}$$

The ensemble average of $\Phi^{(\ell)}$, i.e.,

$$\langle \Phi^{(\ell)}(\mathbf{r}) \rangle = f^{(\ell)} \qquad (\ell = 1, 2), \tag{17}$$

delivers the volume fraction of component material ℓ, which is subject to the constraint $\sum_{\ell=1}^{2} f^{(\ell)} = 1$. As the component materials are treated symmetrically within the SPFT, the estimates of the HCM's constitutive parameters are not restricted to very low or very high volume fractions; instead they are appropriate for arbitrary values of $f^{(\ell)} \in (0, 1)$.

The ensemble average of the product $\Phi^{(\ell)}(\mathbf{r})\Phi^{(\ell)}(\mathbf{r}')$ constitutes a two-point covariance function, relating the points $\mathbf{r}$ and $\mathbf{r}'$. Investigations involving the electromagnetic SPFT have demonstrated that the specific form of the covariance function has only a minor influence on the estimates of HCM constitutive parameters, for a range of physically plausible covariance functions [26]. Here we adopt the physically motivated form [27]

$$\langle \Phi^{(\ell)}(\mathbf{r})\Phi^{(\ell)}(\mathbf{r}')\rangle = \begin{cases} \langle \Phi^{(\ell)}(\mathbf{r})\rangle\langle \Phi^{(\ell)}(\mathbf{r}')\rangle, & |\underline{\underline{U}}^{-1}\cdot(\mathbf{r}-\mathbf{r}')| > L \\ \langle \Phi^{(\ell)}(\mathbf{r})\rangle, & |\underline{\underline{U}}^{-1}\cdot(\mathbf{r}-\mathbf{r}')| \leqslant L, \end{cases} \tag{18}$$

which has been widely used in electromagnetic and elastodynamic SPFT studies. Thus, interactions between pairs of points which are separated by a distance less than $|\underline{\underline{U}}^{-1}\cdot(\mathbf{r}-\mathbf{r}')|$ are taken into account. The correlation length L in equation (18) is required to be much smaller than the associated piezoelectric wavelengths, but larger than the particle size parameter η.

2.3. Comparison material

A homogeneous comparison material provides the initial ansatz for an iterative procedure that delivers a succession of SPFT estimates of the HCM constitutive parameters [18]. Accordingly, the comparison material represents the lowest order SPFT estimate of the HCM. In consonance with the component materials, the comparison material is an orthorhombic $mm2$ piezoelectric material, in general. The piezoelectric constitutive properties of this orthorhombic comparison material (OCM) are encapsulated by its extended stiffness symbol $\breve{C}^{(\mathrm{OCM})}_{lMPq}$ (and its 12×12 matrix equivalent $\underline{\underline{\breve{\mathbf{C}}}}^{(\mathrm{OCM})}$) and extended density symbol $\breve{\rho}^{(\mathrm{OCM})}_{MP}$ (and its 4×4 matrix equivalent $\underline{\underline{\breve{\rho}}}^{(\mathrm{OCM})}$).

In order to establish the spectral Green function for the OCM—which is a key element in the SPFT formulation—we first consider the corresponding extended equation of motion. This may be written in the frequency domain as [28]

$$\breve{C}^{(\mathrm{OCM})}_{lMPq}\partial_l\partial_q\breve{u}_P + \omega^2\breve{u}_M = -\breve{F}_M, \tag{19}$$

where the extended displacement

$$\breve{u}_M = \begin{cases} u_m, & M = m = 1,2,3 \\ \Phi, & P = 4 \end{cases} \tag{20}$$

combines the displacement u_m and electric scalar potential Φ, and the extended body force

$$\breve{F}_M = \begin{cases} F_m, & M = m = 1,2,3 \\ -q, & M = 4 \end{cases} \tag{21}$$

combines the body force F_m and the electric charge q. Following the approach of Zhuck and Lakhtakia [18], the spatial Fourier transformation of equation (19) yields the sought after spectral Green function for the OCM as the 4×4 matrix:

$$\underline{\underline{\mathbf{G}}}^{(\mathrm{OCM})}(\mathbf{k}) = [k^2\underline{\underline{\mathbf{a}}}(\hat{\mathbf{k}}) - \omega^2\underline{\underline{\breve{\rho}}}^{(\mathrm{OCM})}]^{-1}. \tag{22}$$

Herein, the 4×4 matrix $\underline{\underline{\mathbf{a}}}(\hat{\mathbf{k}})$ has entries

$$[\underline{\underline{\mathbf{a}}}(\hat{\mathbf{k}})]_{MP} = \frac{k_s\breve{C}^{(\mathrm{OCM})}_{sMPq}k_q}{k^2}, \tag{23}$$

while $\mathbf{k} = k\hat{\mathbf{k}} \equiv (k_1,k_2,k_3)$ with $\hat{\mathbf{k}} = (\sin\theta\cos\phi, \sin\theta\sin\phi, \cos\theta)$.

As is comprehensively described elsewhere [13–17], the SPFT approach is based upon the asymptotic expansion of a mass operator term. The mass operator is expressed in a renormalized form in order to accommodate relatively strong fluctuations in the constitutive parameters describing the comparison medium and the component materials. In order to remove secular terms from this expansion, the two conditions [18]

$$\left\langle \Phi^{(1)}(\mathbf{r})\xi^{(1)}_{lMPq} + \Phi^{(2)}(\mathbf{r})\xi^{(2)}_{lMPq} \right\rangle = 0, \tag{24}$$

$$\langle \Phi^{(1)}(\mathbf{r})[\breve{\rho}^{(1)} - \breve{\rho}^{(\mathrm{OCM})}]_{MP} + \Phi^{(2)}(\mathbf{r})[\breve{\rho}^{(2)} - \breve{\rho}^{(\mathrm{OCM})}]_{MP} \rangle = 0 \tag{25}$$

are imposed. We note that equation (24) is, in fact, the Bruggeman equation, which has been widely used in electromagnetics for the past 70 years [29]. In equation (24), the quantities

$$\xi^{(\ell)}_{lMPq} = \left(\breve{C}^{(\ell)}_{lMSt} - \breve{C}^{(\mathrm{OCM})}_{lMSt}\right)\eta^{(\ell)}_{StPq} \qquad (\ell = 1, 2), \tag{26}$$

where $\eta^{(\ell)}_{StPq}$ is given implicitly through

$$\breve{S}^{(\ell)}_{Pq} = \eta^{(\ell)}_{PqSt} f^{(\ell)}_{St}, \tag{27}$$

$$f^{(\ell)}_{Tj} = \breve{S}^{(\ell)}_{Tj} + W_{TjlM}\left(\breve{C}^{(\ell)}_{lMPq} - \breve{C}^{(\mathrm{OCM})}_{lMPq}\right)\breve{S}^{(\ell)}_{Pq} \tag{28}$$

with the renormalization tensor

$$W_{PstU} = \begin{cases} \dfrac{1}{8\pi}\displaystyle\int_0^{2\pi} \mathrm{d}\phi \int_0^{\pi} \mathrm{d}\theta\, \frac{\sin\theta}{(\underline{\underline{\mathbf{U}}}^{-1}\cdot\hat{\mathbf{k}})\cdot(\underline{\underline{\mathbf{U}}}^{-1}\cdot\hat{\mathbf{k}})} & \\ \quad\times(\underline{\underline{\mathbf{U}}}^{-1}\cdot\hat{\mathbf{k}})_t\{(\underline{\underline{\mathbf{U}}}^{-1}\cdot\hat{\mathbf{k}})_s[\underline{\underline{\mathbf{a}}}^{-1}(\underline{\underline{\mathbf{U}}}^{-1}\cdot\hat{\mathbf{k}})]_{pU} & \\ \quad+(\underline{\underline{\mathbf{U}}}^{-1}\cdot\hat{\mathbf{k}})_p[\underline{\underline{\mathbf{a}}}^{-1}(\underline{\underline{\mathbf{U}}}^{-1}\cdot\hat{\mathbf{k}})]_{sU}\}, & P = p = 1, 2, 3 \\ \dfrac{1}{8\pi}\displaystyle\int_0^{2\pi} \mathrm{d}\phi \int_0^{\pi} \mathrm{d}\theta\,\sin\theta\, \frac{(\underline{\underline{\mathbf{U}}}^{-1}\cdot\hat{\mathbf{k}})_t(\underline{\underline{\mathbf{U}}}^{-1}\cdot\hat{\mathbf{k}})_s[\underline{\underline{\mathbf{a}}}^{-1}(\underline{\underline{\mathbf{U}}}^{-1}\cdot\hat{\mathbf{k}})]_{pU}}{(\underline{\underline{\mathbf{U}}}^{-1}\cdot\hat{\mathbf{k}})\cdot(\underline{\underline{\mathbf{U}}}^{-1}\cdot\hat{\mathbf{k}})}, & P = 4. \end{cases} \tag{29}$$

Upon substituting equations (26)–(28) into equation (24), exploiting equation (17), and after some algebraic manipulations, we obtain

$$f^{(1)}[(\underline{\underline{\breve{\mathbf{C}}}}^{(1)} - \underline{\underline{\breve{\mathbf{C}}}}^{(\mathrm{OCM})})^\dagger + \underline{\underline{\mathbf{W}}}]^\dagger + f^{(2)}[(\underline{\underline{\breve{\mathbf{C}}}}^{(2)} - \underline{\underline{\breve{\mathbf{C}}}}^{(\mathrm{OCM})})^\dagger + \underline{\underline{\mathbf{W}}}]^\dagger = \underline{\underline{\mathbf{0}}}_{12\times 12}, \tag{30}$$

wherein the 12×12 matrix equivalent of W_{RstU} (namely, $\underline{\underline{\mathbf{W}}}$) has been introduced and † denotes the matrix operation defined in appendix A. The OCM stiffness matrix may be extracted from (30) as

$$\underline{\underline{\breve{\mathbf{C}}}}^{(\mathrm{OCM})} = \underline{\underline{\breve{\mathbf{C}}}}^{(1)} + f^{(2)}[\underline{\underline{\boldsymbol{\tau}}} + (\underline{\underline{\breve{\mathbf{C}}}}^{(2)} - \underline{\underline{\breve{\mathbf{C}}}}^{(\mathrm{OCM})})\cdot\underline{\underline{\mathbf{W}}}]^\dagger\cdot(\underline{\underline{\breve{\mathbf{C}}}}^{(1)} - \underline{\underline{\breve{\mathbf{C}}}}^{(2)}), \tag{31}$$

where $\underline{\underline{\boldsymbol{\tau}}}$ is the 12×12 matrix representation of the extended identity $\tau_{rSTu} = \tau_{RstU}$, as described in appendix A. By standard numerical procedures, such as the Jacobi method [30], the nonlinear relation (31) is solved for $\underline{\underline{\breve{\mathbf{C}}}}^{(\mathrm{OCM})}$.

After combining equation (17) with equation (25), it follows immediately that the OCM density is the volume average of the densities of the component materials '1' and '2'; i.e.,

$$\underline{\underline{\breve{\boldsymbol{\rho}}}}^{(\mathrm{OCM})} = f^{(1)}\underline{\underline{\breve{\boldsymbol{\rho}}}}^{(1)} + f^{(2)}\underline{\underline{\breve{\boldsymbol{\rho}}}}^{(2)}. \tag{32}$$

2.4. Second-order SPFT

Now that the lowest order (or zeroth-order) SPFT estimate—namely, the comparison medium—has been introduced, let us turn to higher order SPFT estimates of the HCM's constitutive parameters. A fundamental characteristic feature of the SPFT is that the first-order estimate is identical to the zeroth order, whereas the second-order correction is nontrivial [14, 16]. For the orthorhombic $mm2$ piezoelectric scenario considered here, the second-order estimates of the HCM-extended stiffness and density symbols are derived in exactly the same way as the corresponding orthotropic elastodynamic results [18]. Furthermore, using the matrix-vector notation introduced in section 2.1, the piezoelectric estimates may be expressed as three-dimensional integrals which are formally identical to the corresponding elastodynamic estimates. Therefore, we have

$$\begin{aligned}\breve{C}^{(\mathrm{SPFT})}_{lMPq} = \breve{C}^{(\mathrm{OCM})}_{lMPq} &- \frac{\omega^2}{2}\int \mathrm{d}^3k\,\frac{k_t}{k^2}\,B^{lMrs}_{tUPq}(\mathbf{k})[\underline{\underline{\breve{\rho}}}^{(\mathrm{OCM})}]_{XY}[\underline{\underline{\mathbf{G}}}^{(\mathrm{OCM})}(\mathbf{k})]_{YU}\\ &\times \{k_s[\underline{\underline{\mathbf{a}}}^{-1}(\hat{\mathbf{k}})]_{rX} + k_r[\underline{\underline{\mathbf{a}}}^{-1}(\hat{\mathbf{k}})]_{sX}\}\\ &- \frac{\omega^2}{2}\int \mathrm{d}^3k\,\frac{k_t}{k^2}\,B^{lM4s}_{tUPq}(\mathbf{k})[\underline{\underline{\breve{\rho}}}^{(\mathrm{OCM})}]_{XY}[\underline{\underline{\mathbf{G}}}^{(\mathrm{OCM})}(\mathbf{k})]_{YU}\{k_s[\underline{\underline{\mathbf{a}}}^{-1}(\hat{\mathbf{k}})]_{4X}\}\end{aligned} \tag{33}$$

and

$$\breve{\rho}^{(\mathrm{SPFT})}_{MP} = \breve{\rho}^{(\mathrm{OCM})}_{MP} + \omega^2\int \mathrm{d}^3k\,B_{MSUP}(\mathbf{k})[\underline{\underline{\mathbf{G}}}^{(\mathrm{OCM})}(\mathbf{k})]_{SU}. \tag{34}$$

The symbols $B^{lMRs}_{tUPq}(\mathbf{k})$ and $B_{MSUP}(\mathbf{k})$ represent the spectral covariance functions given as

$$\left.\begin{aligned} B^{lMNs}_{tUPq}(\mathbf{k}) &= \frac{\big(\xi^{(2)}_{lMNs}-\xi^{(1)}_{lMNs}\big)\big(\xi^{(2)}_{tUPq}-\xi^{(1)}_{tUPq}\big)}{8\pi^3}\int \mathrm{d}^3R\,\Gamma(\mathbf{R})\exp(-\mathrm{i}\mathbf{k}\cdot\mathbf{R})\\ B_{MSUP}(\mathbf{k}) &= \frac{\big(\breve{\rho}^{(2)}_{MS}-\breve{\rho}^{(1)}_{MS}\big)\big(\breve{\rho}^{(2)}_{UP}-\breve{\rho}^{(1)}_{UP}\big)}{8\pi^3}\int \mathrm{d}^3R\,\Gamma(\mathbf{R})\exp(-\mathrm{i}\mathbf{k}\cdot\mathbf{R})\end{aligned}\right\} \tag{35}$$

with

$$\begin{aligned}\Gamma(\mathbf{R}) = \Gamma(\mathbf{r}-\mathbf{r}') &= \langle\Phi^{(1)}(\mathbf{r})\Phi^{(1)}(\mathbf{r}')\rangle - \langle\Phi^{(1)}(\mathbf{r})\rangle\langle\Phi^{(1)}(\mathbf{r}')\rangle\\ &\equiv \langle\Phi^{(2)}(\mathbf{r})\Phi^{(2)}(\mathbf{r}')\rangle - \langle\Phi^{(2)}(\mathbf{r})\rangle\langle\Phi^{(2)}(\mathbf{r}')\rangle.\end{aligned} \tag{36}$$

In order to make the integrals in the expressions for $\breve{C}^{(\mathrm{SPFT})}_{lMPq}$ and $\breve{\rho}^{(\mathrm{SPFT})}_{MP}$ presented in equations (33) and (34) numerically tractable, we simplify them as follows. Let us begin with the integral on the right sides of equations (35). Upon implementing the step function-shaped covariance function (18), we find

$$\int \mathrm{d}^3R\,\Gamma(\mathbf{R})\exp(-\mathrm{i}\mathbf{k}\cdot\mathbf{R}) = \int_{|\mathbf{R}|\leqslant L}\mathrm{d}^3R\,\exp[-\mathrm{i}(\underline{\underline{\mathbf{U}}}\cdot\mathbf{k})\cdot\mathbf{R}]. \tag{37}$$

Thereby, the expressions for $B^{lMRs}_{tUPq}(\mathbf{k})$ and $B_{MSUP}(\mathbf{k})$ reduce to

$$\left.\begin{aligned} B^{lMRs}_{tUPq}(\mathbf{k}) &= \frac{f^{(1)}f^{(2)}\big(\xi^{(2)}_{lMRs}-\xi^{(1)}_{lMRs}\big)\big(\xi^{(2)}_{tUPq}-\xi^{(1)}_{tUPq}\big)}{2(\pi k\sigma)^2}\left[\frac{\sin(k\sigma L)}{k\sigma} - L\cos(k\sigma L)\right]\\ B_{MSUP}(\mathbf{k}) &= \frac{f^{(1)}f^{(2)}\big(\breve{\rho}^{(2)}_{MS}-\breve{\rho}^{(1)}_{MS}\big)\big(\breve{\rho}^{(2)}_{UP}-\breve{\rho}^{(1)}_{UP}\big)}{2(\pi k\sigma)^2}\left[\frac{\sin(k\sigma L)}{k\sigma} - L\cos(k\sigma L)\right]\end{aligned}\right\}, \tag{38}$$

wherein the scalar function

$$\sigma \equiv \sigma(\theta,\phi) = \sqrt{a^2\sin^2\theta\cos^2\phi + b^2\sin^2\theta\sin^2\phi + c^2\cos^2\theta} \tag{39}$$

is introduced.

Now we turn to the integrals in (33) and (34). In analogy with the corresponding expression for the elastodynamic SPFT [19], the spectral Green function $\underline{\underline{\mathbf{G}}}^{(\mathrm{OCM})}(\mathbf{k})$ may be conveniently expressed as

$$\underline{\underline{\mathbf{G}}}^{(\mathrm{OCM})}(\mathbf{k}) = \frac{\underline{\underline{\mathbf{D}}}(\mathbf{k})}{\Delta(\mathbf{k})}, \tag{40}$$

where the 4×4 matrix function

$$\underline{\underline{\mathbf{D}}}(\mathbf{k}) = \mathrm{adj}[k^2 \underline{\underline{\mathbf{a}}}(\hat{\mathbf{k}}) - \omega^2 \underline{\underline{\breve{\rho}}}^{(\mathrm{OCM})}] \tag{41}$$

and the scalar function

$$\begin{aligned}\Delta(k) = {} & k^8 \det[\underline{\underline{\mathbf{a}}}(\hat{\mathbf{k}})] - \mathrm{tr}\{\mathrm{adj}[k^2 \underline{\underline{\mathbf{a}}}(\hat{\mathbf{k}})] \cdot \omega^2 \underline{\underline{\breve{\rho}}}^{(\mathrm{OCM})}\} - k^2\, \mathrm{tr}[\mathrm{adj}(\omega^2 \underline{\underline{\breve{\rho}}}^{(\mathrm{OCM})}) \cdot \underline{\underline{\mathbf{a}}}(\hat{\mathbf{k}})] \\ & + k^4 (\mathrm{tr}\{[\underline{\underline{\mathbf{a}}}(\hat{\mathbf{k}})]_{44} [\underline{\underline{\mathbf{a}}}^{\sharp}(\hat{\mathbf{k}}) \cdot \mathrm{adj}(\omega^2 \underline{\underline{\breve{\rho}}}^{\sharp})]\} - [\underline{\underline{\mathbf{a}}}(\hat{\mathbf{k}})]_{41} [\underline{\underline{\mathbf{a}}}(\hat{\mathbf{k}})]_{14} [\mathrm{adj}(\omega^2 \underline{\underline{\breve{\rho}}}^{\sharp})]_{11} \\ & - [\underline{\underline{\mathbf{a}}}(\hat{\mathbf{k}})]_{42} [\underline{\underline{\mathbf{a}}}(\hat{\mathbf{k}})]_{24} [\mathrm{adj}(\omega^2 \underline{\underline{\breve{\rho}}}^{\sharp})]_{22} - [\underline{\underline{\mathbf{a}}}(\hat{\mathbf{k}})]_{31} [\underline{\underline{\mathbf{a}}}(\hat{\mathbf{k}})]_{13} [\mathrm{adj}(\omega^2 \underline{\underline{\breve{\rho}}}^{\sharp})]_{33})\end{aligned} \tag{42}$$

with the 3×3 matrixes $\underline{\underline{\mathbf{a}}}^{\sharp}$ and $\underline{\underline{\breve{\rho}}}^{\sharp}$ having entries

$$\left.\begin{aligned}[\underline{\underline{\mathbf{a}}}^{\sharp}]_{pq} &= [\underline{\underline{\mathbf{a}}}(\hat{\mathbf{k}})]_{pq} \\ [\underline{\underline{\breve{\rho}}}^{\sharp}]_{pq} &= [\underline{\underline{\breve{\rho}}}^{(\mathrm{OCM})}]_{pq}\end{aligned}\right\} \qquad (p, q = 1, 2, 3). \tag{43}$$

Through exploiting equations (38) and (40), the integrals in equations (33) and (34) with respect to k can be evaluated by means of calculus of residues: the roots of $\Delta(\mathbf{k}) = 0$ give rise to seven poles in the complex-k plane, located at $k = 0, \pm p_1, \pm p_2, \pm p_3$, which are chosen such that p_n $(n = 1, 2, 3)$ lie in the upper-half of the complex plane. From equation (42), we find that the nonzero poles satisfy

$$p_1 = \sqrt{P_A - \frac{1}{3}\left(\frac{2^{1/3} P_B}{P_C} - \frac{P_C}{2^{1/3}}\right)}, \tag{44}$$

$$p_2 = \sqrt{P_A + \frac{1}{3}\left(\frac{(1 + \mathrm{i}\sqrt{3}) P_B}{2^{2/3} P_C} - \frac{(1 - \mathrm{i}\sqrt{3}) P_C}{2^{4/3}}\right)}, \tag{45}$$

$$p_3 = \sqrt{P_A + \frac{1}{3}\left(\frac{(1 - \mathrm{i}\sqrt{3}) P_B}{2^{2/3} P_C} - \frac{(1 + \mathrm{i}\sqrt{3}) P_C}{2^{4/3}}\right)}, \tag{46}$$

wherein

$$P_A = \frac{\omega^2\, \mathrm{tr}\{\mathrm{adj}[\underline{\underline{\mathbf{a}}}(\hat{\mathbf{k}})] \cdot \underline{\underline{\breve{\rho}}}^{(\mathrm{OCM})}\}}{3 \det[\underline{\underline{\mathbf{a}}}(\hat{\mathbf{k}})]}, \tag{47}$$

$$P_B = -C_A^2 + 3 C_B, \tag{48}$$

$$P_C = \left[P_D + \left(4 P_B^3 + P_D^2\right)^{1/2}\right]^{1/3}, \tag{49}$$

$$P_D = -2 C_A^3 + 9 C_A C_B - 27 C_C, \tag{50}$$

with

$$C_A = \frac{-\omega^2\, \mathrm{tr}\{\mathrm{adj}[\underline{\underline{\mathbf{a}}}(\hat{\mathbf{k}})] \cdot \underline{\underline{\breve{\rho}}}^{(\mathrm{OCM})}\}}{\det[\underline{\underline{\mathbf{a}}}(\hat{\mathbf{k}})]}, \tag{51}$$

$$C_B = \frac{\omega^4}{\det[\underline{\underline{\mathbf{a}}}(\hat{\mathbf{k}})]}\{[\underline{\underline{\mathbf{a}}}(\hat{\mathbf{k}})]_{44}\,\mathrm{tr}[\underline{\underline{\mathbf{a}}}^\sharp(\hat{\mathbf{k}})\cdot\mathrm{adj}(\underline{\underline{\breve{\rho}}}^\sharp)] + [\underline{\underline{\mathbf{a}}}(\hat{\mathbf{k}})]_{41}[\underline{\underline{\mathbf{a}}}(\hat{\mathbf{k}})]_{14}[\mathrm{adj}(\underline{\underline{\breve{\rho}}}^{(\mathrm{OCM})})]_{11}$$
$$+[\underline{\underline{\mathbf{a}}}(\hat{\mathbf{k}})]_{42}[\underline{\underline{\mathbf{a}}}(\hat{\mathbf{k}})]_{24}[\mathrm{adj}(\underline{\underline{\breve{\rho}}}^{(\mathrm{OCM})})]_{22} + [\underline{\underline{\mathbf{a}}}(\hat{\mathbf{k}})]_{43}[\underline{\underline{\mathbf{a}}}(\hat{\mathbf{k}})]_{34}[\mathrm{adj}(\underline{\underline{\breve{\rho}}}^{(\mathrm{OCM})})]_{33}\}, \tag{52}$$

$$C_C = \frac{-\omega^6\,\mathrm{tr}\{\mathrm{adj}[\underline{\underline{\breve{\rho}}}^{(\mathrm{OCM})}]\cdot\underline{\underline{\mathbf{a}}}(\hat{\mathbf{k}})\}}{\det[\underline{\underline{\mathbf{a}}}(\hat{\mathbf{k}})]}. \tag{53}$$

Thus, by application of the Cauchy residue theorem [31], the SPFT estimates are delivered in terms of two-dimensional integrals as

$$\breve{C}^{(\mathrm{SPFT})}_{lMPq} = \breve{C}^{(\mathrm{OCM})}_{lMPq} + \frac{\omega^2 f^{(1)} f^{(2)}}{4\pi i}\int_{\phi=0}^{2\pi}\int_{\theta=0}^{\pi} \mathrm{d}\phi\,\mathrm{d}\theta\,\frac{k_t\sin\theta}{(k\sigma)^2\det[\underline{\underline{\mathbf{a}}}(\hat{\mathbf{k}})]}[\underline{\underline{\breve{\rho}}}^{(\mathrm{OCM})}]_{XY}[\underline{\underline{\mathbf{b}}}(\hat{\mathbf{k}})]_{YU}$$
$$\times\left(\left\{\xi^{(2)}_{lMrs} - \xi^{(1)}_{lMrs}\right\}\{k_s[\underline{\underline{\mathbf{a}}}^{-1}(\hat{\mathbf{k}})]_{rX} + k_r[\underline{\underline{\mathbf{a}}}^{-1}(\hat{\mathbf{k}})]_{sX}\}\right.$$
$$\left.+\left\{\xi^{(2)}_{lm4s} - \xi^{(1)}_{lm4s}\right\}\{k_s[\underline{\underline{\mathbf{a}}}^{-1}(\hat{\mathbf{k}})]_{4X}\}\right)\left(\xi^{(2)}_{tUPq} - \xi^{(1)}_{tUPq}\right) \tag{54}$$

and

$$\breve{\rho}^{(\mathrm{SPFT})}_{MP} = \breve{\rho}^{(\mathrm{OCM})}_{MP} - \frac{\omega^2 f^{(1)} f^{(2)}\left(\breve{\rho}^{(2)}_{MS} - \breve{\rho}^{(1)}_{MS}\right)\left(\breve{\rho}^{(2)}_{UP} - \breve{\rho}^{(1)}_{UP}\right)}{2\pi\mathrm{i}}$$
$$\times\int_{\phi=0}^{2\pi}\int_{\theta=0}^{\pi}\mathrm{d}\phi\,\mathrm{d}\theta\,\frac{\sin\theta}{\det[\underline{\underline{\mathbf{a}}}(\hat{\mathbf{k}})]}[\underline{\underline{\mathbf{b}}}(\hat{\mathbf{k}})]_{SU}, \tag{55}$$

where the 4×4 matrix

$$\underline{\underline{\mathbf{b}}}(\hat{\mathbf{k}}) = \frac{1}{2\mathrm{i}}\left\{\frac{\mathrm{e}^{\mathrm{i}L\sigma p_1}\,\underline{\underline{\mathbf{D}}}(p_1\underline{\underline{\mathbf{U}}}\cdot\hat{\mathbf{k}})}{\sigma p_1^4\left(p_1^2-p_2^2\right)\left(p_1^2-p_3^2\right)}(1-\mathrm{i}L\sigma p_1) - \frac{\mathrm{e}^{\mathrm{i}L\sigma p_2}\,\underline{\underline{\mathbf{D}}}(p_2\underline{\underline{\mathbf{U}}}\cdot\hat{\mathbf{k}})}{\sigma p_2^4\left(p_1^2-p_2^2\right)\left(p_2^2-p_3^2\right)}(1-\mathrm{i}L\sigma p_2)\right.$$
$$+\frac{\mathrm{e}^{\mathrm{i}L\sigma p_3}\,\underline{\underline{\mathbf{D}}}(p_3\underline{\underline{\mathbf{U}}}\cdot\hat{\mathbf{k}})}{\sigma p_3^4\left(p_2^2-p_3^2\right)\left(p_1^2-p_3^2\right)}(1-\mathrm{i}L\sigma p_3)$$
$$\left.-\frac{1}{\sigma p_1^2p_2^2p_3^2}\left[\underline{\underline{\mathbf{D}}}(\mathbf{0})\left(\frac{1}{p_1^2}+\frac{1}{p_2^2}+\frac{1}{p_3^2}+\frac{\sigma^2L^2}{2}\right)+\frac{1}{2}\frac{\partial^2}{\partial k^2}\underline{\underline{\mathbf{D}}}(\mathbf{0})\right]\right\}. \tag{56}$$

The expressions for the second-order SPFT estimates $\breve{C}^{(\mathrm{SPFT})}_{lMPq}$ and $\breve{\rho}^{(\mathrm{SPFT})}_{MP}$ in equations (54) and (55) may be evaluated by standard numerical methods [32]. Note that the location of poles of the integrands in equations (33) and (34) is independent of the shape parameters $\{a, b, c\}$. Accordingly, the integration with respect k is independent of the shape of the particle, in contrast to the integrations with respect to the angular coordinates θ and ϕ.

It is particularly noteworthy that $\breve{C}^{(\mathrm{SPFT})}_{lMPq}$ and $\breve{\rho}^{(\mathrm{SPFT})}_{MP}$ are complex valued for $L > 0$, even when the corresponding quantities for the component materials, i.e., $\breve{C}^{(\ell)}_{lMPq}$ and $\breve{\rho}^{(\ell)}_{MP}$ ($\ell = 1, 2$), are real valued. This reflects the fact that the SPFT accommodates attenuation due to scattering losses [16]. Within the frequency domain, the imaginary parts of the constitutive parameters indicate a phase lag between applied fields and the material response to these applied fields. For example, the imaginary part of the complex-valued density term indicates a phase lag between an applied force and displacement. From energy considerations, the imaginary part of the extended compliance matrix, namely [21]

$$\underline{\underline{\breve{\mathbf{M}}}}^{(\mathrm{SPFT})} = \begin{pmatrix} (\underline{\underline{\mathbf{C}}}^{(\mathrm{SPFT})})^\ddagger & (\underline{\underline{\mathbf{C}}}^{(\mathrm{SPFT})})^\ddagger\cdot(\underline{\underline{\mathbf{e}}}^{(\mathrm{SPFT})})^T \\ \underline{\underline{\mathbf{e}}}^{(\mathrm{SPFT})}\cdot(\underline{\underline{\mathbf{C}}}^{(\mathrm{SPFT})})^\ddagger & \underline{\underline{\epsilon}}^{(\mathrm{SPFT})} + \underline{\underline{\mathbf{e}}}^{(\mathrm{SPFT})}\cdot(\underline{\underline{\mathbf{C}}}^{(\mathrm{SPFT})})^\ddagger\cdot(\underline{\underline{\mathbf{e}}}^{(\mathrm{SPFT})})^T \end{pmatrix} \tag{57}$$

is required to be positive definite for passive materials [33]. The constitutive matrixes $\underline{\underline{\mathbf{C}}}^{(\mathrm{SPFT})}$, $\underline{\underline{\mathbf{e}}}^{(\mathrm{SPFT})}$ and $\underline{\underline{\epsilon}}^{(\mathrm{SPFT})}$ on the right side of equation (57) are related to the extended stiffness matrix $\underline{\underline{\breve{\mathbf{C}}}}^{(\mathrm{SPFT})}$ (and thereby to the extended stiffness symbol $\breve{C}^{(\mathrm{SPFT})}_{lMPq}$) per equation (7), and ‡ denotes the 9×9 matrix operation analogous to the † operation described in appendix A, which we define elsewhere [19].

Let us note that convergence of the SPFT scheme has been demonstrated at the second-order level of approximation for the electromagnetic constitutive parameters of a very general class of linear HCMs [22, 23]. Accordingly, we do not consider the third-order SPFT here.

3. Numerical results

3.1. Preliminaries

In order to illustrate the theory presented in section 2, let us now consider a representative numerical example. A comparison for the SPFT estimate of the HCM constitutive parameters is provided by the corresponding results computed using the Mori–Tanaka formalism [8, 11, 24, 25]. In the case of orthorhombic $mm2$ piezoelectric component materials, the Mori–Tanaka estimate of the extended stiffness matrix for the HCM is given by [12]

$$\underline{\underline{\breve{\mathbf{C}}}}^{(\mathrm{MT})} = \underline{\underline{\breve{\mathbf{C}}}}^{(1)} + f^{(2)}(\underline{\underline{\breve{\mathbf{C}}}}^{(2)} - \underline{\underline{\breve{\mathbf{C}}}}^{(1)}) \cdot \underline{\underline{\mathbf{B}}}^{(\mathrm{MT})} \cdot [f^{(1)}\underline{\underline{\tau}} + f^{(2)}\underline{\underline{\mathbf{B}}}^{(\mathrm{MT})}]^{\dagger}, \tag{58}$$

where the 12×12 matrix

$$\underline{\underline{\mathbf{B}}}^{(\mathrm{MT})} = [\underline{\underline{\tau}} + \underline{\underline{\mathbf{S}}}^{(\mathrm{Esh})} \cdot (\underline{\underline{\breve{\mathbf{C}}}}^{(1)})^{\dagger} \cdot (\underline{\underline{\breve{\mathbf{C}}}}^{(2)} - \underline{\underline{\breve{\mathbf{C}}}}^{(1)})]^{\dagger} \tag{59}$$

with $\underline{\underline{\mathbf{S}}}^{(\mathrm{Esh})}$ being the 12×12 matrix representation of the Eshelby tensor [7, 9, 34]. Details on evaluating $\underline{\underline{\mathbf{S}}}^{(\mathrm{Esh})}$ can be found in appendix B.

In the following, we present the numerical evaluation of the 12×12 extended stiffness matrix of the HCM, namely $\underline{\underline{\breve{\mathbf{C}}}}^{(\mathrm{HCM})}$, as estimated by the lowest order SPFT (i.e., HCM = OCM), the second-order SPFT (i.e., HCM = SPFT) and the Mori–Tanaka formalism (i.e., HCM = MT). The matrix $\underline{\underline{\breve{\mathbf{C}}}}^{(\mathrm{HCM})}$ has the form represented in equation (7). The second-order SPFT density tensor $\breve{\rho}^{(\mathrm{SPFT})}_{MP}$ is also evaluated; the numerical evaluation of the lowest order SPFT density $\breve{\rho}^{(\mathrm{OCM})}_{MP}$ need not be presented here as this quantity is simply the volume average of the densities of the component materials. For consistency with an earlier elastodynamic SPFT study [19], an angular frequency of $\omega = 2\pi \times 10^6\,\mathrm{s}^{-1}$ was selected for all second-order SPFT computations, but we note that our results are not sensitive to ω.

The eccentricities of the ellipsoidal component particles are specified by the shape parameters $\{a, b, c\}$, per equations (14) and (15). In the following we consider both spherical and ellipsoidal particles. For both cases the HCM exhibits the orthorhombic $mm2$ structure described in section 2.1. More complex symmetries arise in scenarios wherein the principal axes of the component particles are not aligned with the coordinate axes. The limiting cases corresponding to very thin needle and very flat disk particle shapes can be approached numerically, but the integral expressions for W_{PstU}, $\breve{C}^{(\mathrm{SPFT})}_{lMPq}$ and $\breve{\rho}^{(\mathrm{SPFT})}_{MP}$ are not amenable to exact evaluation for orthorhombic $mm2$ materials in these cases.

To allow direct comparison with results from previous studies [12], component material '1' was taken to be the piezoelectric material polyvinylidene fluoride (PVDF) while component material '2' was taken to be the thermoplastic polyimide LaRC-SI, which has no piezoelectric properties. The stiffness constitutive parameters of the component materials are tabulated in table 1. The nonzero piezoelectric constitutive parameters of PVDF are: $e_{113} \equiv e_{31} = 0.024$, $e_{223} \equiv e_{32} = 0.001$ and $e_{333} \equiv e_{33} = -0.027$ in units of C m^{-2}. The

Table 1. The stiffness constitutive parameters of the component materials in units of GPa (after [12]).

Stiffness parameter	PVDF (GPa)	LaRC-SI (GPa)
$C_{1111} \equiv C_{11}$	3.8	8.1
$C_{1122} \equiv C_{12}$	1.9	5.4
$C_{1133} \equiv C_{13}$	1.0	5.4
$C_{2222} \equiv C_{22}$	3.2	8.1
$C_{2233} \equiv C_{23}$	0.9	5.4
$C_{3333} \equiv C_{33}$	1.2	8.1
$C_{2323} \equiv C_{44}$	0.7	1.4
$C_{1313} \equiv C_{55}$	0.9	1.4
$C_{1212} \equiv C_{66}$	0.9	1.4

dielectric constitutive parameters of PVDF are $\epsilon_{11} = 7.4$, $\epsilon_{22} = 9.6$ and $\epsilon_{33} = 7.6$, whereas those of LaRC-SI are $\epsilon_{11} = \epsilon_{22} = \epsilon_{33} = 2.8$, all in units of $\epsilon_0 = 8.854 \times 10^{-12}$ F m^{-1} (the permittivity of free space). Lastly, the densities of PVDF and LaRC-SI are 1750 and 1376, respectively, in units of kg m^{-3}.

3.2. Lowest order SPFT

We begin by considering the lowest order SPFT estimates of the HCM constitutive parameters. In figure 2, components of the HCM-extended stiffness matrix $\underline{\underline{\breve{\mathbf{C}}}}^{(\mathrm{HCM})}$, as computed using the lowest order SPFT and the Mori–Tanaka formalism, are plotted as functions of volume fraction $f^{(2)}$ for the case where the component particles are spherical (i.e., $a = b = c$). Plots of only a representative selection of the components of $\underline{\underline{\breve{\mathbf{C}}}}^{(\mathrm{HCM})}$ are presented in figure 2; plots for those components which are not presented in figure 2 are qualitatively similar to those that are presented. Only relatively minor differences between the lowest order SPFT estimates and the Mori–Tanaka estimates are observed, with the differences between the two being greatest for mid-range values of $f^{(2)}$. Plots for both the SPFT and Mori–Tanaka estimates are necessarily constrained by the limits

$$\lim_{f^{(2)}\to 0} \underline{\underline{\breve{\mathbf{C}}}}^{(\mathrm{HCM})} = \underline{\underline{\breve{\mathbf{C}}}}^{(1)}, \qquad \lim_{f^{(2)}\to 1} \underline{\underline{\breve{\mathbf{C}}}}^{(\mathrm{HCM})} = \underline{\underline{\breve{\mathbf{C}}}}^{(2)}. \tag{60}$$

The corresponding graphs for the cases where the components particles are described by the shape parameters $\{a/c = 5, b/c = 1.5\}$ and $\{a/c = 10, b/c = 2\}$ are provided in figures 3 and 4, respectively. A comparison of figures 2–4 reveals that the differences between the lowest order SPFT and Mori–Tanaka estimates are accentuated as the component particles become more eccentric in shape, especially at mid-range values of $f^{(2)}$ for the piezoelectric parameters and the dielectric parameters. A notable feature in figures 3 and 4 is that the graph of $[\underline{\underline{\breve{\mathbf{C}}}}^{(\mathrm{MT})}]_{1,12}$ undergoes a sign change as $f^{(2)}$ increases whereas the graph of $[\underline{\underline{\breve{\mathbf{C}}}}^{(\mathrm{OCM})}]_{1,12}$ does not. There is no theoretical barrier to prevent these piezoelectric constitutive parameters from changing sign, provided that the imaginary part of the extended compliance matrix $\underline{\underline{\breve{\mathbf{M}}}}^{(\mathrm{SPFT})}$ remains positive definite—indeed, we note that for PVDF $e_{31,32}$ are positive valued whereas e_{33} is negative valued.

3.3. Second-order SPFT estimate

Now let us turn to the second-order SPFT estimates of the HCM constitutive parameters. We considered these quantities as functions of $\bar{k}L$, where $\bar{k}$ is an approximate upper bound on the

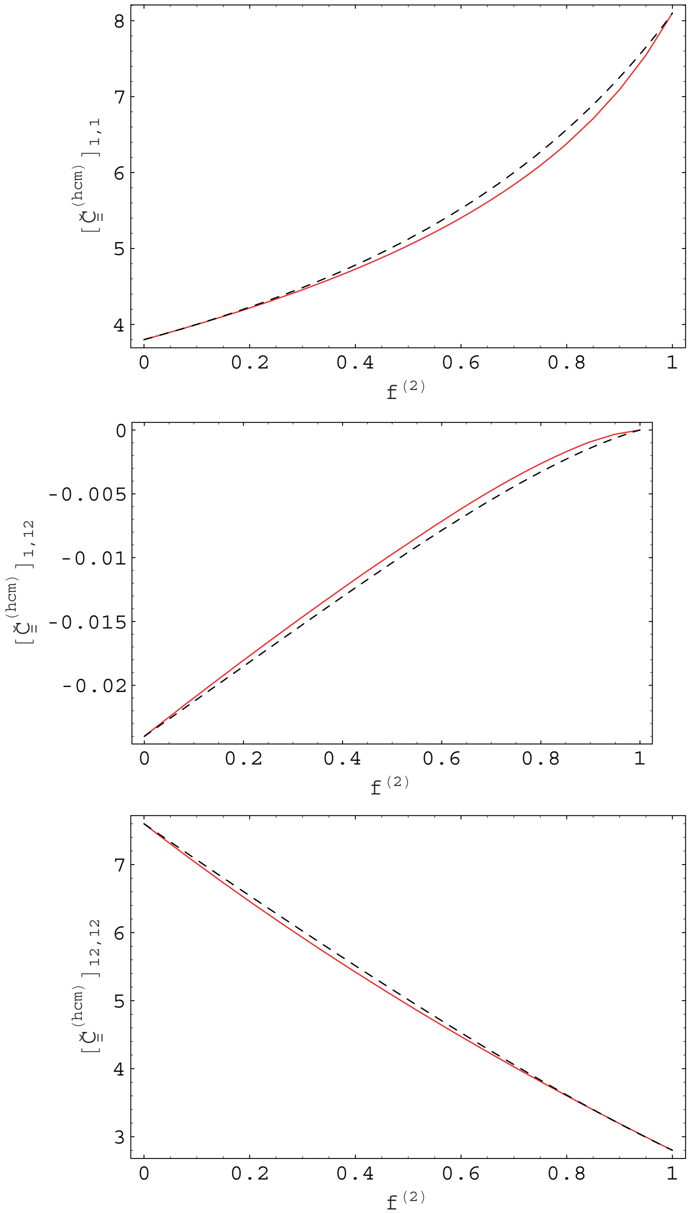

Figure 2. Plots of $[\underline{\underline{\check{\mathbf{C}}}}^{(\mathrm{HCM})}]_{1,1}$ (in GPa), $[\underline{\underline{\check{\mathbf{C}}}}^{(\mathrm{HCM})}]_{1,12}$ (in C m^{-2}) and $(1/\epsilon_0)[\underline{\underline{\check{\mathbf{C}}}}^{(\mathrm{hcm})}]_{12,12}$ as estimated using the lowest order SPFT (i.e., $\overline{\mathrm{H}}$CM = OCM) (black, dashed curves) and the Mori–Tanaka formalism (i.e., HCM = MT) (red, solid curves) versus the volume fraction of component material '2'. Component material '1' is PVDF and component material '2' is LaRC-SI, as described in section 3.1. The component materials are distributed as spheres (i.e., $a = b = c$).

wavenumbers supported by the HCM, as estimated by [19]

$$\bar{k} = \frac{\omega}{2}\left(\sqrt{\frac{\bar{\rho}}{\bar{\lambda} + 2\bar{\mu}}} + \sqrt{\frac{\bar{\rho}}{\bar{\mu}}}\right), \tag{61}$$

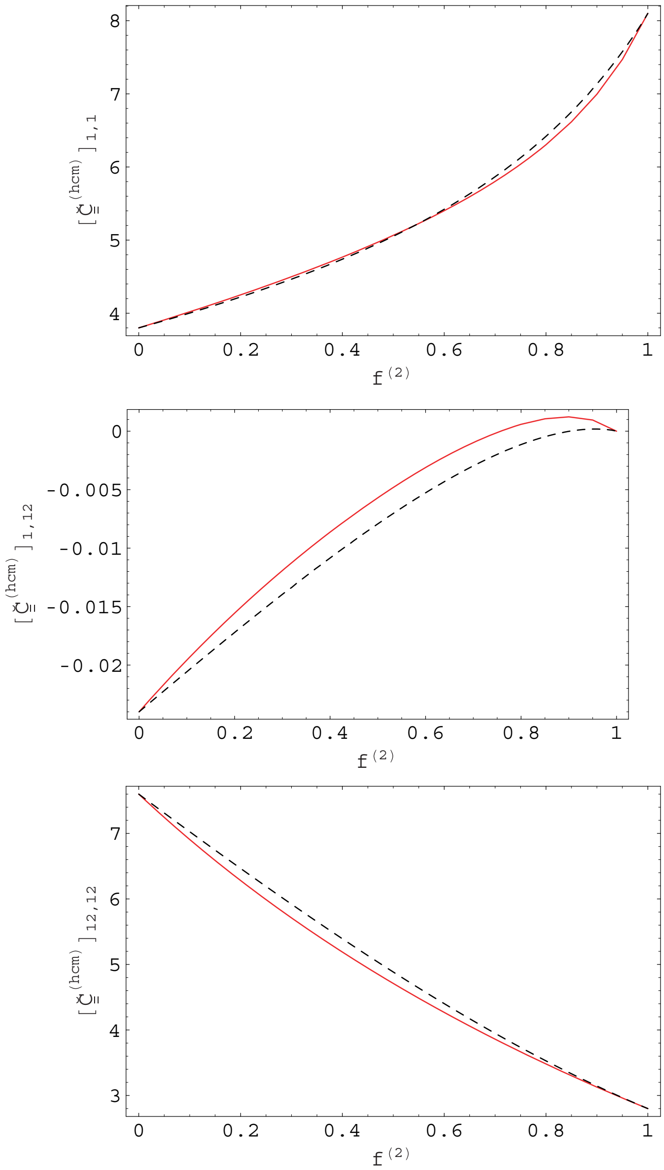

Figure 3. As figure 2 but with the component materials distributed as ellipsoids with ($a/c = 5$ and $b/c = 1.5$).

wherein

$$\left.\begin{aligned}\bar{\lambda} &= \frac{1}{6}\sum_{\ell=1}^{2}(|[\underline{\underline{\mathbf{C}}}^{(\ell)}]_{12}| + |[\underline{\underline{\mathbf{C}}}^{(\ell)}]_{13}| + |[\underline{\underline{\mathbf{C}}}^{(\ell)}]_{23}|)\\ \bar{\mu} &= \frac{1}{6}\sum_{\ell=1}^{2}(|[\underline{\underline{\mathbf{C}}}^{(\ell)}]_{44}| + |[\underline{\underline{\mathbf{C}}}^{(\ell)}]_{55}| + |[\underline{\underline{\mathbf{C}}}^{(\ell)}]_{66}|)\\ \bar{\rho} &= \frac{1}{2}\sum_{\ell=1}^{2}\rho^{(\ell)}\end{aligned}\right\} \tag{62}$$

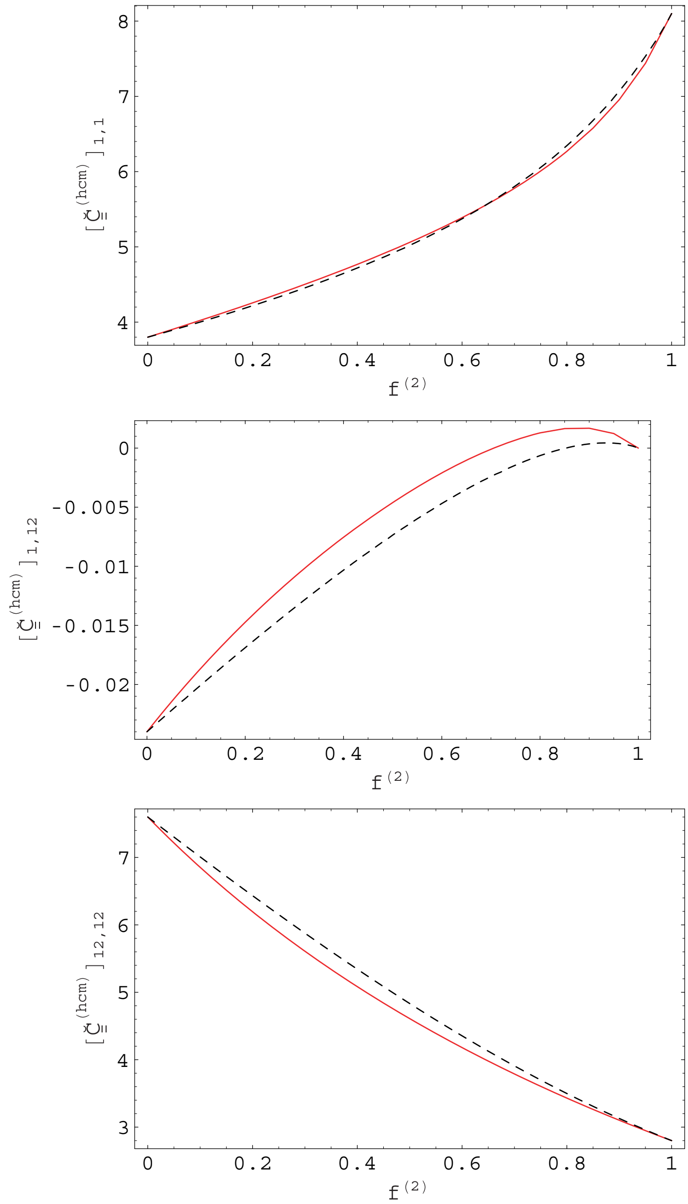

Figure 4. As figure 2 but with the component materials distributed as ellipsoids with ($a/c = 10$ and $b/c = 2$).

and L is the correlation length associated with the two-point covariance function (18). In figure 5, the real and imaginary parts of the components of $\tilde{\underline{\underline{\mathbf{C}}}}^{(\mathrm{SPFT})} = \breve{\underline{\underline{\mathbf{C}}}}^{(\mathrm{SPFT})} - \breve{\underline{\underline{\mathbf{C}}}}^{(\mathrm{OCM})}$ are plotted against $\bar{k}L$ for $f^{(2)} = 0.5$. The values of the shape parameters $\{a, b, c\}$ correspond to those used in the calculations for figures 2–4. As in section 3.2, only a representative selection of the components of $\tilde{\underline{\underline{\mathbf{C}}}}^{(\mathrm{SPFT})}$ are plotted in figure 5; the graphs for those components that are not represented in figure 5 are qualitatively similar to the graphs which do appear.

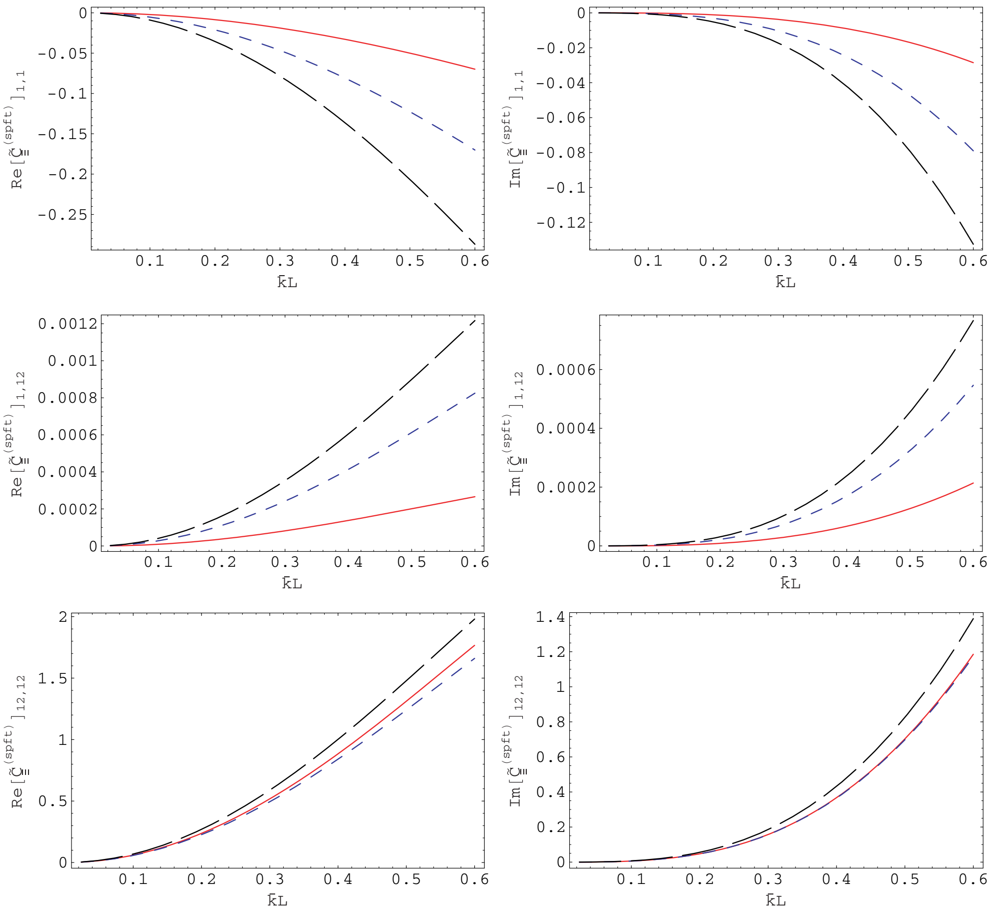

Figure 5. Plots of the real and imaginary parts of the second-order SPFT estimates $[\underline{\underline{\tilde{\mathbf{C}}}}^{(\mathrm{SPFT})}]_{1,1}$ (in GPa), $[\underline{\underline{\tilde{\mathbf{C}}}}^{(\mathrm{SPFT})}]_{1,12}$ (in C m^{-2}) and $(10^3/\epsilon_0)[\underline{\underline{\tilde{\mathbf{C}}}}^{(\mathrm{SPFT})}]_{12,12}$, where $\underline{\underline{\tilde{\mathbf{C}}}}^{(\mathrm{SPFT})} = \underline{\underline{\breve{\mathbf{C}}}}^{(\mathrm{SPFT})} - \underline{\underline{\breve{\mathbf{C}}}}^{(\mathrm{OCM})}$, versus $\breve{k}L$, with $f^{(2)} = 0.5$. The results from the spherical particle (i.e., $a = b = c = 1$) case (red, solid line) are plotted alongside the cases with elliptical particles with $a = 5, b = 1.5, c = 1$ (blue, short-dashed line) and $a = 10, b = 2, c = 1$ (black, long-dashed line).

The second-order corrections to the lowest order SPFT estimates are observed in figure 5 to grow exponentially in magnitude as the correlation length increases from zero. Furthermore, the magnitudes of both the real and imaginary parts of $\underline{\underline{\breve{\mathbf{C}}}}^{(\mathrm{SPFT})}$ generally grow faster with increasing correlation length when the component particles are more eccentric in shape. At $L = 0$, the second-order and lowest order SPFT estimates coincide. While the second-order corrections are relatively small compared to the lowest order SPFT estimates, a highly significant feature of the second-order corrections is that these are complex valued with nonzero imaginary parts, even though $\underline{\underline{\breve{\mathbf{C}}}}^{(1,2)}$ and $\underline{\underline{\breve{\mathbf{C}}}}^{(\mathrm{OCM})}$ are purely real valued. We note that for all computations the imaginary part of the extended compliance matrix $\underline{\underline{\breve{\mathbf{M}}}}^{(\mathrm{SPFT})}$ was found to be positive definite, which corresponds to positive loss [33]. Thus, the emergence of nonzero imaginary parts of $\underline{\underline{\breve{\mathbf{C}}}}^{(\mathrm{SPFT})}$ indicates that the HCM has acquired an effectively dissipative nature, despite the component materials being nondissipative. The effective dissipation

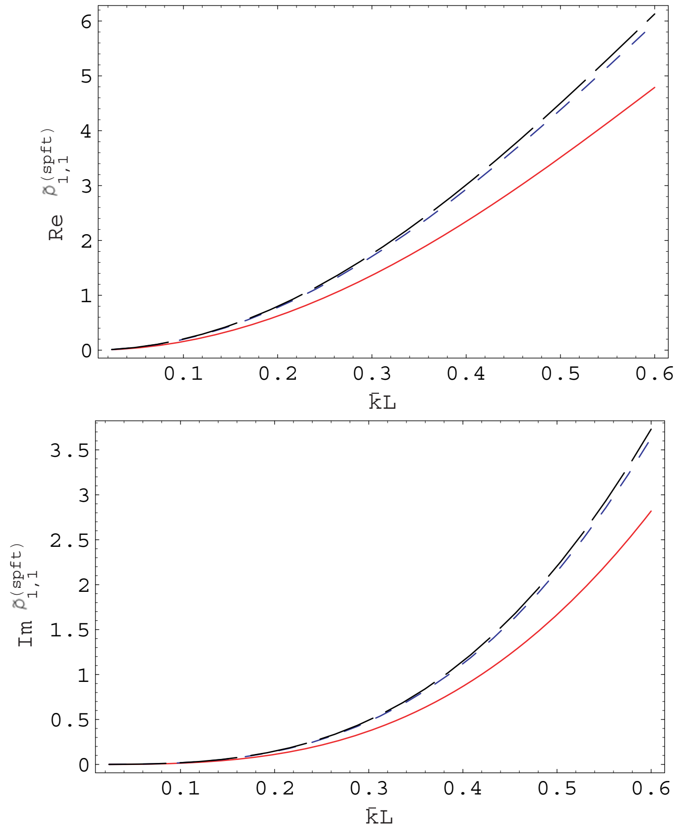

Figure 6. As figure 5 but with the real and imaginary parts of $[\underline{\underline{\tilde{\rho}}}^{(\mathrm{SPFT})}]_{11}$ (in kg m^{-3}), where $\underline{\underline{\tilde{\rho}}}^{(\mathrm{SPFT})} = \underline{\underline{\breve{\rho}}}^{(\mathrm{SPFT})} - \underline{\underline{\breve{\rho}}}^{(\mathrm{OCM})}$, plotted as functions of $\bar{k}L$, with $f^{(2)} = 0.5$.

is attributed to attenuation via scattering losses, since the second-order SPFT takes into account interactions between spatially distinct scattering particles via the two-point covariance function (18). As the correlation length increases, the number of scattering particles that can mutually interact also increases, thereby increasing the scattering loss per unit volume. The attenuation arising from these scattering losses is exhibited whenever the correlation length is nonzero.

Finally, we turn to the second-order SPFT estimate of the HCM density. The real and imaginary parts of the matrix entry $[\underline{\underline{\tilde{\rho}}}^{(\mathrm{SPFT})}]_{11}$, wherein $\underline{\underline{\tilde{\rho}}}^{(\mathrm{SPFT})} = \underline{\underline{\breve{\rho}}}^{(\mathrm{SPFT})} - \underline{\underline{\breve{\rho}}}^{(\mathrm{OCM})}$ are plotted as functions of $\bar{k}L$ in figure 6. The corresponding graphs for $[\underline{\underline{\tilde{\rho}}}^{(\mathrm{SPFT})}]_{22}$ and $[\underline{\underline{\tilde{\rho}}}^{(\mathrm{SPFT})}]_{33}$ are much the same as those for $[\underline{\underline{\tilde{\rho}}}^{(\mathrm{SPFT})}]_{11}$ but with minor differences in magnitudes. The second-order SPFT estimates of the HCM density exhibit characteristics similar to those of the corresponding HCM stiffness, piezoelectric and dielectric constitutive parameters. That is, $\lim_{L\to 0} \rho^{(\mathrm{SPFT})}_{aa} = \rho^{(\mathrm{OCM})}$ and $\left|\tilde{\rho}^{(\mathrm{SPFT})}_{aa}\right| \ll |\rho^{(\mathrm{OCM})}|$ for $a = 1, 2$ and 3. Also, the differences between $\underline{\underline{\breve{\rho}}}^{(\mathrm{SPFT})}$ and $\underline{\underline{\breve{\rho}}}^{(\mathrm{OCM})}$ increase exponentially as the correlation length increases, and this effect is most accentuated when the component particles are most eccentric in shape. The matrix entries $[\underline{\underline{\tilde{\rho}}}^{(\mathrm{SPFT})}]_{ab}$ where $a \neq b$ are null valued. Thus, we find that the second-order SPFT estimate of the HCM density is influenced by the statistical distribution of the component materials in much the same way as the corresponding HCM stiffness, piezoelectric and dielectric constitutive parameters, with the imaginary parts of the complex-valued density parameters representing attenuation due to scattering losses.

Are the zeroth-order or second-order SPFT estimates of the HCM constitutive parameters closer to the Mori–Tanaka estimates? Since the second-order SPFT estimates are complex valued with nonzero imaginary parts, whereas the zeroth-order SPFT and Mori–Tanaka estimates are real valued, the zeroth-order SPFT estimates and the Mori–Tanaka estimates are qualitatively closer. From the numerical results presented here (and others not presented here), there is no obvious trend when only the real parts of the second-order SPFT estimates are considered: for some constitutive parameters the real parts of the second-order SPFT estimates are closer to those of the Mori–Tanaka formalism, but not for others.

The relatively small difference in magnitude between the zeroth-order SPFT estimates of the HCM stiffness, piezoelectric, dielectric and density constitutive parameters and those of the second-order SPFT suggests that the SPFT scheme converges rapidly at the second-order level of approximation. This finding is consistent with previous studies wherein convergence of electromagnetic SPFT was established at the second-order level of approximation [22, 23].

Finally in this section, we remark that an anisotropic density—which should be interpreted as an effective density—also crops up in the second-order elastodynamic SPFT for orthotropic HCMs [19], as well as in other homogenization scenarios [35, 36].

4. Closing remarks

The linear SPFT has been fully developed for the case of orthorhombic $mm2$ piezoelectric HCMs, based on component materials distributed as oriented ellipsoidal particles. The multifunctionality of such HCMs is central to the notion of metamaterials [5]. The second-order estimates of the HCM constitutive parameters are expressed in terms of numerically tractable two-dimensional integrals, for a specific choice of two-point covariance function. This theoretical result further extends the application of the SPFT in the homogenization of complex composites, effectively bridging the elastodynamic SPFT for orthotropic HCMs [18, 19] and the electromagnetic SPFT for anisotropic dielectric HCMs [37, 38]. Furthermore, the path has now been cleared toward the development of the SPFT for piezoelectric/piezomagnetic HCMs [39], with bianisotropic electromagnetic properties [16]. Let us remark that the mathematical description of piezoelectric HCMs presented herein also extends to electrokinetic processes [40].

From our theoretical considerations and representative numerical studies, the following conclusions were drawn.

- The lowest order SPFT estimate of the stiffness, piezoelectric and dielectric properties of the HCM are qualitatively similar to those estimates provided by the Mori–Tanaka formalism.
- Differences between the estimates of the lowest order SPFT and the Mori–Tanaka formalism are greatest at mid-range values of the volume fraction, and accentuated when the component particles are eccentric in shape.
- The second-order SPFT provides a correction to the lowest order estimate of the HCM constitutive properties. The magnitude of this correction is generally larger when the component particles are more eccentric in shape and vanishes as the correlation length tends to zero.
- While the correction provided by the second-order SPFT is relatively small in magnitude, it is highly significant as it indicates attenuation due to scattering loss.

By accommodating higher order statistics, the SPFT approach to homogenization introduces a length scale to the description of the HCM. The relationship between this description and other generalized continuum models such as the Cosserat model, wherein an intrinsic material length scale is introduced by admitting rotational degrees of freedom to the constituent particles making up the continuum [41–44], is a matter to be explored in the future.

We have found that the lowest order SPFT estimates of the HCM constitutive parameters are qualitatively similar to those provided by the Mori–Tanaka formalism, whereas the second-order SPFT estimates are fundamentally different owing to higher order distributional statistics of the component materials being taken into account. However, the acid test of the effectiveness of the second-order SPFT predictions should be provided by appropriate experimental data, which are not currently available. A notable limitation of the SPFT approach to homogenization—which is shared by most other conventional approaches—is that the size of the component material particles are not taken into account. Progress has been made in this area recently for the electromagnetic SPFT [45, 46]; similar developments for the elastodynamic and piezoelectric SPFT are keenly awaited.

Acknowledgments

The authors thank two anonymous referees for their helpful remarks which led to improvements in the manuscript. AJD is supported by an *Engineering and Physical Sciences Research Council* (UK) studentship.

Appendix A

The extended symbol $\breve{A}_{aMPq}$ $(a, q \in \{1,2,3\}, M, P \in \{1,2,3,4\})$ may be conveniently represented by the 12×12 matrix with entries $[\underline{\underline{\breve{\mathbf{A}}}}]_{\gamma\kappa}$ $(\gamma, \kappa \in [1, 12])$, upon replacing the index pair aM with γ and the index pair Pq with κ. For the most general 12×12 matrix encountered in this paper, which has the form

$$\underline{\underline{\breve{\mathbf{A}}}} = \begin{pmatrix} A_{1,1} & A_{1,2} & A_{1,3} & 0 & 0 & 0 & 0 & 0 & 0 & 0 & 0 & A_{1,12} \\ A_{2,1} & A_{2,2} & A_{2,3} & 0 & 0 & 0 & 0 & 0 & 0 & 0 & 0 & A_{2,12} \\ A_{3,1} & A_{3,2} & A_{3,3} & 0 & 0 & 0 & 0 & 0 & 0 & 0 & 0 & A_{3,12} \\ 0 & 0 & 0 & A_{4,4} & 0 & 0 & A_{4,4} & 0 & 0 & 0 & A_{4,11} & 0 \\ 0 & 0 & 0 & 0 & A_{5,5} & 0 & 0 & A_{5,5} & 0 & A_{5,10} & 0 & 0 \\ 0 & 0 & 0 & 0 & 0 & A_{6,6} & 0 & 0 & A_{6,6} & 0 & 0 & 0 \\ 0 & 0 & 0 & A_{4,4} & 0 & 0 & A_{4,4} & 0 & 0 & 0 & A_{4,11} & 0 \\ 0 & 0 & 0 & 0 & A_{5,5} & 0 & 0 & A_{5,5} & 0 & A_{5,10} & 0 & 0 \\ 0 & 0 & 0 & 0 & 0 & A_{6,6} & 0 & 0 & A_{6,6} & 0 & 0 & 0 \\ 0 & 0 & 0 & 0 & A_{10,5} & 0 & 0 & A_{10,5} & 0 & A_{10,10} & 0 & 0 \\ 0 & 0 & 0 & A_{11,4} & 0 & 0 & A_{11,4} & 0 & 0 & 0 & A_{11,11} & 0 \\ A_{12,1} & A_{12,2} & A_{12,3} & 0 & 0 & 0 & 0 & 0 & 0 & 0 & 0 & A_{12,12} \end{pmatrix}, \tag{A.1}$$

the correspondence between the extended symbol indexes and the matrix indexes is provided in table A.1. The scheme presented in table A.1 also relates the extended symbol $\breve{t}_{aM}$ to the corresponding column 12-vector entries $[\breve{\mathbf{t}}]_{\gamma}$.

Table A.1. Conversion between the extended symbol and matrix notation.

aM or Pq	γ or κ	aM or Pq	γ or κ	aM or Pq	γ or κ	aM or Pq	γ or κ
11	1	23 or 32	4	23 or 32	7	14 or 41	10
22	2	13 or 31	5	13 or 31	8	24 or 42	11
33	3	12 or 21	6	12 or 21	9	34 or 43	12

We introduce the matrix $\underline{\underline{\breve{\mathbf{A}}}}^\dagger$ which plays a role similar to the matrix inverse insofar as

$$\underline{\underline{\breve{\mathbf{A}}}}^\dagger \cdot \underline{\underline{\breve{\mathbf{A}}}} = \underline{\underline{\breve{\mathbf{A}}}} \cdot \underline{\underline{\breve{\mathbf{A}}}}^\dagger = \underline{\underline{\tau}}. \tag{A.2}$$

Herein,

$$\underline{\underline{\tau}} = \begin{pmatrix} \underline{\underline{\mathbf{I}}} & \underline{\underline{\mathbf{0}}}_{3\times3} & \underline{\underline{\mathbf{0}}}_{3\times3} & \underline{\underline{\mathbf{0}}}_{3\times3} \\ \underline{\underline{\mathbf{0}}}_{3\times3} & \frac{1}{2}\underline{\underline{\mathbf{I}}} & \frac{1}{2}\underline{\underline{\mathbf{I}}} & \underline{\underline{\mathbf{0}}}_{3\times3} \\ \underline{\underline{\mathbf{0}}}_{3\times3} & \frac{1}{2}\underline{\underline{\mathbf{I}}} & \frac{1}{2}\underline{\underline{\mathbf{I}}} & \underline{\underline{\mathbf{0}}}_{3\times3} \\ \underline{\underline{\mathbf{0}}}_{3\times3} & \underline{\underline{\mathbf{0}}}_{3\times3} & \underline{\underline{\mathbf{0}}}_{3\times3} & \underline{\underline{\mathbf{I}}} \end{pmatrix} \tag{A.3}$$

is the 12×12 matrix representation of the extended identity symbol, with $\underline{\underline{\mathbf{I}}}$ being the 3×3 identity matrix, and we have

$$\underline{\underline{\breve{\mathbf{A}}}} \cdot \underline{\underline{\tau}} = \underline{\underline{\tau}} \cdot \underline{\underline{\breve{\mathbf{A}}}} = \underline{\underline{\breve{\mathbf{A}}}}. \tag{A.4}$$

The matrix $\underline{\underline{\breve{\mathbf{A}}}}^\dagger$ has the form

$$\underline{\underline{\breve{\mathbf{A}}}}^\dagger = \begin{pmatrix}
\dagger_{1,1} & \dagger_{1,2} & \dagger_{1,3} & 0 & 0 & 0 & 0 & 0 & 0 & 0 & 0 & \dagger_{1,12} \\
\dagger_{2,1} & \dagger_{2,2} & \dagger_{2,3} & 0 & 0 & 0 & 0 & 0 & 0 & 0 & 0 & \dagger_{2,12} \\
\dagger_{3,1} & \dagger_{3,2} & \dagger_{3,3} & 0 & 0 & 0 & 0 & 0 & 0 & 0 & 0 & \dagger_{3,12} \\
0 & 0 & 0 & \frac{\dagger_{4,4}}{2} & 0 & 0 & \frac{\dagger_{4,4}}{2} & 0 & 0 & 0 & \dagger_{4,11} & 0 \\
0 & 0 & 0 & 0 & \frac{\dagger_{5,5}}{2} & 0 & 0 & \frac{\dagger_{5,5}}{2} & 0 & \dagger_{5,10} & 0 & 0 \\
0 & 0 & 0 & 0 & 0 & \frac{\dagger_{6,6}}{2} & 0 & 0 & \frac{\dagger_{6,6}}{2} & 0 & 0 & 0 \\
0 & 0 & 0 & \frac{\dagger_{4,4}}{2} & 0 & 0 & \frac{\dagger_{4,4}}{2} & 0 & 0 & 0 & \dagger_{4,11} & 0 \\
0 & 0 & 0 & 0 & \frac{\dagger_{5,5}}{2} & 0 & 0 & \frac{\dagger_{5,5}}{2} & 0 & \dagger_{5,10} & 0 & 0 \\
0 & 0 & 0 & 0 & 0 & \frac{\dagger_{6,6}}{2} & 0 & 0 & \frac{\dagger_{6,6}}{2} & 0 & 0 & 0 \\
0 & 0 & 0 & 0 & \dagger_{10,5} & 0 & 0 & \dagger_{10,5} & 0 & \dagger_{10,10} & 0 & 0 \\
0 & 0 & 0 & \dagger_{11,4} & 0 & 0 & \dagger_{11,4} & 0 & 0 & 0 & \dagger_{11,11} & 0 \\
\dagger_{12,1} & \dagger_{12,2} & \dagger_{12,3} & 0 & 0 & 0 & 0 & 0 & 0 & 0 & 0 & \dagger_{12,12}
\end{pmatrix}, \tag{A.5}$$

with entries

$$\dagger_{1,1} = (-A_{12,3}A_{2,2}A_{3,12} + A_{12,2}A_{2,3}A_{3,12} + A_{12,3}A_{2,12}A_{3,2} - A_{12,12}A_{2,3}A_{3,2} \\ - A_{12,2}A_{2,12}A_{3,3} + A_{12,12}A_{2,2}A_{3,3})/\Lambda, \tag{A.6}$$

$$\dagger_{1,2} = (A_{1,2}A_{12,3}A_{3,12} - A_{12,2}A_{1,3}A_{3,12} - A_{1,12}A_{12,3}A_{3,2} + A_{12,12}A_{1,3}A_{3,2} \\ - A_{1,2}A_{12,12}A_{3,3} + A_{1,12}A_{12,2}A_{3,3})/\Lambda, \tag{A.7}$$

$$\dagger_{1,3} = (-A_{1,2}A_{12,3}A_{2,12} + A_{12,2}A_{1,3}A_{2,12} + A_{1,12}A_{12,3}A_{2,2} - A_{12,12}A_{1,3}A_{2,2} \\ + A_{1,2}A_{12,12}A_{2,3} - A_{1,12}A_{12,2}A_{2,3})/\Lambda, \tag{A.8}$$

$$\dagger_{2,1} = (-A_{12,3}A_{2,12}A_{3,1} + A_{12,12}A_{2,3}A_{3,1} + A_{12,3}A_{2,1}A_{3,12} - A_{12,1}A_{2,3}A_{3,12} - A_{12,12}A_{2,1}A_{3,3} + A_{12,1}A_{2,12}A_{3,3})/\Lambda, \tag{A.9}$$

$$\dagger_{2,2} = (A_{1,12}A_{12,3}A_{3,1} - A_{12,12}A_{1,3}A_{3,1} - A_{1,1}A_{12,3}A_{3,12} + A_{12,1}A_{1,3}A_{3,12} - A_{1,12}A_{12,1}A_{3,3} + A_{1,1}A_{12,12}A_{3,3})/\Lambda, \tag{A.10}$$

$$\dagger_{2,3} = (-A_{1,12}A_{12,3}A_{2,1} + A_{12,12}A_{1,3}A_{2,1} + A_{1,1}A_{12,3}A_{2,12} - A_{12,1}A_{1,3}A_{2,12} + A_{1,12}A_{12,1}A_{2,3} - A_{1,1}A_{12,12}A_{2,3})/\Lambda, \tag{A.11}$$

$$\dagger_{3,1} = (A_{12,2}A_{2,12}A_{3,1} - A_{12,12}A_{2,2}A_{3,1} - A_{12,2}A_{2,1}A_{3,12} + A_{12,1}A_{2,2}A_{3,12} + A_{12,12}A_{2,1}A_{3,2} - A_{12,1}A_{2,12}A_{3,2})/\Lambda, \tag{A.12}$$

$$\dagger_{3,2} = (A_{1,2}A_{12,12}A_{3,1} - A_{1,12}A_{12,2}A_{3,1} - A_{1,2}A_{12,1}A_{3,12} + A_{1,1}A_{12,2}A_{3,12} + A_{1,12}A_{12,1}A_{3,2} - A_{1,1}A_{12,12}A_{3,2})/\Lambda, \tag{A.13}$$

$$\dagger_{3,3} = (-A_{1,2}A_{12,12}A_{2,1} + A_{1,12}A_{12,2}A_{2,1} + A_{1,2}A_{12,1}A_{2,12} - A_{1,1}A_{12,2}A_{2,12} - A_{1,12}A_{12,1}A_{2,2} + A_{1,1}A_{12,12}A_{2,2})/\Lambda, \tag{A.14}$$

$$\dagger_{4,4} = \frac{A_{11,11}}{2(A_{11,11}A_{4,4} - A_{4,11}A_{11,4})}, \tag{A.15}$$

$$\dagger_{5,5} = \frac{A_{10,10}}{2(A_{10,10}A_{5,5} - A_{5,10}A_{10,5})}, \tag{A.16}$$

$$\dagger_{6,6} = \frac{1}{2A_{6,6}}, \tag{A.17}$$

$$\dagger_{10,10} = \frac{A_{5,5}}{(A_{10,10}A_{5,5} - A_{10,5}A_{5,10})}, \tag{A.18}$$

$$\dagger_{11,11} = \frac{A_{4,4}}{(A_{11,11}A_{4,4} - A_{11,4}A_{4,11})}, \tag{A.19}$$

$$\dagger_{12,12} = (-A_{1,3}A_{2,2}A_{3,1} + A_{1,2}A_{2,3}A_{3,1} + A_{1,3}A_{2,1}A_{3,2} - A_{1,1}A_{2,3}A_{3,2} - A_{1,2}A_{2,1}A_{3,3} + A_{1,1}A_{2,2}A_{3,3})/\Lambda, \tag{A.20}$$

$$\dagger_{1,12} = (A_{1,3}A_{2,2}A_{3,12} - A_{1,2}A_{2,3}A_{3,12} - A_{1,3}A_{2,12}A_{3,2} + A_{1,12}A_{2,3}A_{3,2} + A_{1,2}A_{2,12}A_{3,3} - A_{1,12}A_{2,2}A_{3,3})/\Lambda, \tag{A.21}$$

$$\dagger_{2,12} = (A_{1,3}A_{2,12}A_{3,1} - A_{1,12}A_{2,3}A_{3,1} - A_{1,3}A_{2,1}A_{3,12} + A_{1,1}A_{2,3}A_{3,12} + A_{1,12}A_{2,1}A_{3,3} - A_{1,1}A_{2,12}A_{3,3})/\Lambda, \tag{A.22}$$

$$\dagger_{3,12} = (-A_{1,2}A_{2,12}A_{3,1} + A_{1,12}A_{2,2}A_{3,1} + A_{1,2}A_{2,1}A_{3,12} - A_{1,1}A_{2,2}A_{3,12} - A_{1,12}A_{2,1}A_{3,2} + A_{1,1}A_{2,12}A_{3,2})/\Lambda, \tag{A.23}$$

$$\dagger_{4,11} = \frac{A_{4,11}}{2(A_{11,4}A_{4,11} - A_{11,11}A_{4,4})}, \tag{A.24}$$

$$\dagger_{5,10} = \frac{A_{5,10}}{2(A_{5,10}A_{10,5} - A_{10,10}A_{5,5})}, \tag{A.25}$$

$$\dagger_{12,1} = (A_{12,3}A_{2,2}A_{3,1} - A_{12,2}A_{2,3}A_{3,1} - A_{12,3}A_{2,1}A_{3,2} + A_{12,1}A_{2,3}A_{3,2} + A_{12,2}A_{2,1}A_{3,3} - A_{12,1}A_{2,2}A_{3,3})/\Lambda, \tag{A.26}$$

$$\dagger_{12,2} = (-A_{1,2}A_{12,3}A_{3,1} + A_{12,2}A_{1,3}A_{3,1} + A_{1,1}A_{12,3}A_{3,2} - A_{12,1}A_{1,3}A_{3,2} + A_{1,2}A_{12,1}A_{3,3} - A_{1,1}A_{12,2}A_{3,3})/\Lambda, \tag{A.27}$$

$$\dagger_{12,3} = (A_{1,2}A_{12,3}A_{2,1} - A_{12,2}A_{1,3}A_{2,1} - A_{1,1}A_{12,3}A_{2,2} + A_{12,1}A_{1,3}A_{2,2} - A_{1,2}A_{12,1}A_{2,3} + A_{1,1}A_{12,2}A_{2,3})/\Lambda, \tag{A.28}$$

$$\dagger_{11,4} = \frac{A_{11,4}}{2(A_{11,4}A_{4,11} - A_{11,11}A_{4,4})}, \tag{A.29}$$

$$\dagger_{10,5} = \frac{A_{10,5}}{2(A_{10,5}A_{5,10} - A_{10,10}A_{5,5})}, \tag{A.30}$$

where the scalar

$$\begin{aligned}\Lambda = {} & A_{1,12}A_{12,3}A_{2,2}A_{3,1} - A_{12,12}A_{1,3}A_{2,2}A_{3,1} - A_{1,1}A_{12,3}A_{2,2}A_{3,12} + A_{12,1}A_{1,3}A_{2,2}A_{3,12} \\ & - A_{1,12}A_{12,3}A_{2,1}A_{3,2} + A_{12,12}A_{1,3}A_{2,1}A_{3,2} + A_{1,1}A_{12,3}A_{2,12}A_{3,2} \\ & - A_{12,1}A_{1,3}A_{2,12}A_{3,2} + A_{1,12}A_{12,1}A_{2,3}A_{3,2} - A_{1,1}A_{12,12}A_{2,3}A_{3,2} \\ & - A_{1,12}A_{12,1}A_{2,2}A_{3,3} + A_{1,1}A_{12,12}A_{2,2}A_{3,3} + A_{12,2}(A_{1,3}A_{2,12}A_{3,1} \\ & - A_{1,12}A_{2,3}A_{3,1} - A_{1,3}A_{2,1}A_{3,12} + A_{1,1}A_{2,3}A_{3,12} + A_{1,12}A_{2,1}A_{3,3} \\ & - A_{1,1}A_{2,12}A_{3,3}) + A_{1,2}(-A_{12,3}A_{2,12}A_{3,1} + A_{12,12}A_{2,3}A_{3,1} + A_{12,3}A_{2,1}A_{3,12} \\ & - A_{12,1}A_{2,3}A_{3,12} - A_{12,12}A_{2,1}A_{3,3} + A_{12,1}A_{2,12}A_{3,3}).\end{aligned} \tag{A.31}$$

Appendix B

The extended Eshelby symbol appropriate to orthorhombic $mm2$ piezoelectric materials, distributed as ellipsoidal particles with shape parameters $\{a, b, c\}$, is given by [9, 34]

$$S^{(\mathrm{Esh})}_{MnAb} = \begin{cases} \dfrac{1}{8\pi} C^{(1)}_{sJAb} \displaystyle\int_{-1}^{+1} \mathrm{d}\zeta_3 \int_0^{2\pi} \mathrm{d}\omega [F_{mJsn}(\overline{\vartheta}) + F_{nJsm}(\overline{\vartheta})], & M = m = 1, 2, 3 \\ \dfrac{1}{4\pi} C^{(1)}_{sJAb} \displaystyle\int_{-1}^{+1} \mathrm{d}\zeta_3 \int_0^{2\pi} \mathrm{d}\omega\, F_{4Jsn}(\overline{\vartheta}), & M = 4, \end{cases} \tag{B.1}$$

wherein

$$\left.\begin{array}{llll} F_{MJsn}(\overline{\vartheta}) = \overline{\vartheta}_s \overline{\vartheta}_n K^{-1}_{MJ}, & & K_{JR} = \overline{\vartheta}_s C^{(1)}_{sJRn} \overline{\vartheta}_n & \\ \overline{\vartheta}_1 = \dfrac{\zeta_1}{a}, & \overline{\vartheta}_2 = \dfrac{\zeta_2}{b}, & \overline{\vartheta}_3 = \dfrac{\zeta_3}{c} & \\ \zeta_1 = \left(1 - \zeta_3^2\right)^{1/2} \cos(\omega), & & \zeta_2 = \left(1 - \zeta_3^2\right)^{1/2} \sin(\omega), & \zeta_3 = \zeta_3 \end{array}\right\}. \tag{B.2}$$

The integrals in equations (B.1) can be evaluated using standard numerical methods [32].

The conversion from the extended Eshelby symbol $S^{(\mathrm{Esh})}_{MnAb}$ to the extended Eshelby 12×12 matrix, namely $\underline{\underline{\mathbf{S}}}^{(\mathrm{Esh})}$, follows the scheme described in appendix A.

References

[1] Ting R Y 1986 Evaluation of new piezoelectric composite materials for hydrophone applications *Ferroelectrics* **67** 143–57

[2] Zhang R, Jiang B and Cao W 2001 Elastic, piezoelectric and dielectric properties of multidomain $0.67Pb(Mg_{1/3}Nb_{2/3})O_3 - 0.33PbTiO_3$ single crystals *J. Appl. Phys.* **90** 3471–5

[3] Damjanovic D 1998 Ferroelectric, dielectric and piezoelectric properties of ferroelectric thin films and ceramics *Rep. Prog. Phys.* **61** 1267–324

[4] Swallow L M, Luo J K, Siores E, Patel I and Dodds D 2008 A piezoelectric fibre composite based energy harvesting device for potential wearable applications *Smart Mater. Struct.* **17** 025017

[5] Walser R M 2003 Metamaterials: An introduction *Introduction to Complex Mediums for Optics and Electromagnetics* ed W S Weiglhofer and A Lakhtakia (Bellingham: SPIE) pp 295–316

[6] Mackay T G 2005 Linear and nonlinear homogenized composite mediums as metamaterials *Electromagnetics* **25** 461–81

[7] Eshelby J D 1957 The determination of the elastic field of an ellipsoidal inclusion, and related problems *Proc. R. Soc.* A **241** 376–96

[8] Mori T and Tanaka K 1973 Average stress in matrix and average elastic energy of materials misfitting inclusions *Acta Metall.* **21** 571–4

[9] Dunn M L and Taya M 1993 An analysis of piezoelectric composite materials containing ellipsoidal inhomogeneities *Proc. R. Soc.: Math. Phys. Sci.* **443** 265–87

[10] Huang J H and Kuo W–S 1996 The analysis of piezoelectric/piezomagnetic composite materials containing ellipsoidal inclusions *J. Appl. Phys.* **81** 1378–86

[11] Dunn M L and Taya M 1993 Micromechanics predictions of the effective electroelastic moduli of piezoelectric composites *Int. J. Solids Struct.* **30** 161–75

[12] Odegard G M 2004 Constitutive modeling of piezoelectric polymer composites *Acta Mater.* **52** 5315–30

[13] Ryzhov Yu A and Tamoikin V V 1970 Radiation and propagation of electromagnetic waves in randomly inhomogeneous media *Radiophys. Quantum Electron.* **14** 228–33

[14] Tsang L and Kong J A 1981 Scattering of electromagnetic waves from random media with strong permittivity fluctuations *Radio Sci.* **16** 303–20

[15] Michel B and Lakhtakia A 1995 Strong-property-fluctuation theory for homogenizing chiral particulate composites *Phys. Rev.* E **51** 5701–7

[16] Mackay T G, Lakhtakia A and Weiglhofer W S 2000 Strong-property-fluctuation theory for homogenization of bianisotropic composites: formulation *Phys. Rev.* E **62** 6052–64
Mackay T G, Lakhtakia A and Weiglhofer W S 2001 Strong-property-fluctuation theory for homogenization of bianisotropic composites: formulation *Phys. Rev.* E **63** 049901 (erratum)

[17] Zhuck N P 1996 Strong fluctuation theory for a mean acoustic field in a random fluid medium with statistically anisotropic perturbations *J. Acoust. Soc. Am.* **99** 46–54

[18] Zhuck N P and Lakhtakia A 1999 Effective constitutive properties of a disordered elastic solid medium via the strong–fluctuation approach *Proc R. Soc.* A **455** 543–66

[19] Duncan A D, Mackay T G and Lakhtakia A 2009 On the homogenization of orthotropic elastic composites by the strong–property–fluctuation theory *IMA J. Appl. Math.* (at press) doi:10.1093/imamat/hxp001

[20] Nye J F 1985 *Physical Properties of Crystals* (Oxford: Clarendon)

[21] Auld B A 1990 *Acoustic Fields and Waves in Solids* 2nd edn (Malabar, FL, USA: Krieger Publishing Company)

[22] Mackay T G, Lakhtakia A and Weiglhofer W S 2001 Third-order implementation and convergence of the strong-property-fluctuation theory in electromagnetic homogenisation *Phys. Rev.* E **64** 066616

[23] Cui J and Mackay T G 2007 On convergence of the extended strong-property-fluctuation theory for bianisotropic homogenized composites *Electromagnetics* **27** 495–506

[24] Mura T 1987 *Micromechanics of Defects in Solids* (Dordrecht: Kluwer)

[25] Lakhtakia A 2002 Microscopic model for elastostatic and elastodynamic excitation of chiral sculptured thin films *J. Compos. Mater.* **36** 1277–98

[26] Mackay T G, Lakhtakia A and Weiglhofer W S 2001 Homogenisation of similarly oriented, metallic, ellipsoidal inclusions using the bilocally approximated strong-property-fluctuation theory *Opt. Commun.* **107** 89–95

[27] Tsang L, Kong J A and Newton R W 1982 Application of strong fluctuation random medium theory to scattering of electromagnetic waves from a half-space of dielectric mixture *IEEE Trans. Antennas Propagat.* **30** 292–302

[28] Ma H and Wang B 2005 The scattering of electrostatic waves by an ellipsoidal inclusion in piezoelectric medium *Int. J. Solids Struct.* **42** 4541–54

[29] Bruggeman D A G 1935 Berechnung verschiedener physikalischer Konstanten von heterogenen Substanzen, I. Dielektrizitätskonstanten und Leitfähigkeiten der Mischkörper aus isotropen Substanzen *Ann. Phys. Lpz.* **24** 636–79

[30] Bagnara R 1995 A unified proof for the convergence of Jacobi and Gauss–Seidel methods *SIAM Rev.* **37** 93–7

[31] Kwok Y K 2002 *Applied Complex Variables for Scientists and Engineers* (Cambridge: Cambridge University Press)

[32] Press W H, Flannery B P, Teukolsky S A and Vetterling W T 1992 *Numerical Recipes in Fortran* 2nd edn (Cambridge: Cambridge University Press)

[33] Holland R 1967 Representation of dielectric, elastic, and piezoelectric losses by complex coefficients *IEEE Trans. Sonics Ultrason.* **14** 18–20

[34] Gavazzi A C and Lagoudas D C 1990 On the numerical evaluation of Eshelby's tensor and its application to elastoplastic fibrous composites *Comput. Mech.* **7** 13–9
[35] Willis J R 1985 The nonlocal influence of density variations in a composite *Int. J. Solids Struct.* **21** 805–17
[36] Milton G W 2007 New metamaterials with macroscopic behavior outside that of continuum elastodynamics *New J. Phys.* **9** 359
[37] Genchev Z D 1992 Anisotropic and gyrotropic version of Polder and van Santen's mixing formula *Waves Random Media* **2** 99–110
[38] Zhuck N P 1994 Strong–fluctuation theory for a mean electromagnetic field in a statistically homogeneous random medium with arbitrary anisotropy of electrical and statistical properties *Phys. Rev.* B **50** 15636-45
[39] Nan C–W 1994 Magnetoelectric effect in composites of piezoelectric and piezomagnetic phases *Phys. Rev.* B **50** 6082–8
[40] Adler P M and Mityushev V 2003 Effective medium approximation and exact formulae for electrokinetic phenomena in porous media *J. Phys. A: Math. Gen.* **36** 391–404
[41] Nakamura S, Benedict R L and Lakes R S 1984 Finite element method for orthotropic micropolar elasticity *Int. J. Eng. Sci.* **22** 319–30
[42] Elphinstone M J and Lakhtakia A 1994 Planewave response of an elastic chiral solid slab sandwiched between achiral fluid halfspaces *Proc Ind. Nat. Sci. Acad.* A **60** 593–605
[43] Elphinstone M J and Lakhtakia A 1994 Plane-wave response of an elastic chiral solid slab sandwiched between achiral solid half-spaces *J. Acoust. Soc. Am.* **95** 617–27
[44] Forest S, Dendieve R and Canova G R 1999 Estimating the overall properties of heterogeneous Cosserat materials *Modelling Simul. Mater. Sci. Eng.* **7** 829–40
[45] Cui J and Mackay T G 2007 Depolarization regions of nonzero volume in bianisotropic homogenized composites *Waves Random Complex Media* **17** 269–81
[46] Mackay T G 2008 On extended homogenization formalisms for nanocomposites *J. Nanophotonics* **2** 021850